Recipes for spin-based quantum computing



2005 Nanotechnology 16 R27

(http://iopscience.iop.org/0957-4484/16/4/R01)

INSTITUTE OF PHYSICS PUBLISHING NANOTECHNOLOGY
Nanotechnology **16** (2005) R27–R49 doi:10.1088/0957-4484/16/4/R01

**TUTORIAL**

# Recipes for spin-based quantum computing

**Veronica Cerletti, W A Coish, Oliver Gywat and Daniel Loss**

Department of Physics and Astronomy, University of Basel, Klingelbergstrasse 82, 4056 Basel, Switzerland

Received 1 December 2004, in final form 6 January 2005
Published 25 February 2005
Online at stacks.iop.org/Nano/16/R27

**Abstract**

Technological growth in the electronics industry has historically been measured by the number of transistors that can be crammed onto a single microchip. Unfortunately, all good things must come to an end; spectacular growth in the number of transistors on a chip requires spectacular reduction of the transistor size. For electrons in semiconductors, the laws of quantum mechanics take over at the nanometre scale, and the conventional wisdom for progress (transistor cramming) must be abandoned. This realization has stimulated extensive research on ways to exploit the *spin* (in addition to the orbital) degree of freedom of the electron, giving birth to the field of *spintronics*. Perhaps the most ambitious goal of spintronics is to realize complete control over the quantum mechanical nature of the relevant spins. This prospect has motivated a race to design and build a spintronic device capable of complete control over its quantum mechanical state, and ultimately, performing computations: a quantum computer.

In this tutorial we summarize past and very recent developments which point the way to spin-based quantum computing in the solid state. After introducing a set of basic requirements for any quantum computer proposal, we offer a brief summary of some of the many theoretical proposals for solid-state quantum computers. We then focus on the Loss–DiVincenzo proposal for quantum computing with the spins of electrons confined to quantum dots. There are many obstacles to building such a quantum device. We address these, and survey recent theoretical, and then experimental progress in the field. To conclude the tutorial, we list some as-yet unrealized experiments, which would be crucial for the development of a quantum dot quantum computer.

(Some figures in this article are in colour only in the electronic version)

## 1. Introduction

The fields of semiconductor physics and electronics have been successfully combined for many years. The invention of the transistor meant a revolution for electronics and has led to significant development of semiconductor physics and its industry. More recently, the use of the spin degree of freedom of electrons, as well as the charge, has attracted great interest [1, 2]. In addition to applications for spin electronics (spintronics) in conventional devices, for instance based on the giant magneto-resistance effect [3] and spin-polarized field-effect transistors [4], there are applications that exploit the quantum coherence of the spin. This was encouraged by ground-breaking experiments that showed coherent spin transport over long distances in semiconductors and long electron-spin dephasing times, on the order of 100 ns [5, 6]. In addition, spin-polarized carrier injection from magnetic to non-magnetic semiconductors has been demonstrated [7, 8]. Since the electron spin is a two-level system, it is a natural candidate for the realization of a quantum bit (qubit) [9]. A

  

qubit is the basic unit of information in quantum computation, a discipline which attempts to radically improve the performance of computers by exploiting the quantum properties of the system used as hardware. The confinement of electrons in semiconductor structures like quantum dots allows for better control and isolation of the electron spin from its environment. Control and isolation are important issues to consider for the design of a quantum computer.

The field of quantum computing was born in the 1980s, motivated by the miniaturization of electronic devices. Moore's-law predictions on the exponential growth of the transistor density in microchips raises the question of the possible future direction of the electronics industry. In particular, since small ($\sim$nm) systems are governed by the laws of quantum mechanics, nanoscale hardware components must show quantum behaviour. Since computers are built up from these electronic components, this leads to the idea of quantum computers. A different approach brought Richard Feynman to the concept of quantum computing [10]. The simulation of the dynamics of quantum systems on conventional computers is a hard task, meaning that the computational resources needed to simulate a quantum system increase exponentially with its size; the states of a quantum system are represented as elements in a Hilbert space, and therefore, the dimension of the space needed to describe the state of $n$ qubits is $2^n$. Thus, the simulation of $n$ qubits requires an exponential number ($2^n$) of classical bits. Feynman's idea was that this problem could be solved by simulating the object of study with a system of the same nature; in this case it implies the use of a quantum device to simulate a quantum system.

The efficient solution of problems that were previously considered intractable has aroused some interest. Researchers have begun thinking about how to exploit the quantum properties of a system to perform calculations. Following early work by David Deutsch on the power of universal quantum computing [11], one of the first practical quantum algorithms was presented by David Deutsch and Richard Jozsa in 1992 [12]. The problem it solves is very simple (it determines whether a function is constant or balanced), but it showed for the first time an advantage in using quantum mechanics for computing. In 1994 quantum computation captured world-wide attention, as Peter Shor presented his quantum algorithm for the prime factorization of integers [13]. This had a significant impact due to the striking advantage of this algorithm with respect to its classical counterparts. The time required to factor a number $N$ on a classical computer with currently known algorithms grows exponentially with the number of digits $\log N$ ($\propto e^{(\log N)^{\alpha}}$), while in the case of Shor's algorithm the growth is bounded by a polynomial ($\propto (\log N)^{\alpha}$) [14]. In addition to this fundamental breakthrough in computational complexity, Shor's algorithm also has potential practical relevance; the difficulty of the factorization problem is the key to the security of cryptographic codes. These codes include the RSA (Rivest, Shamir, and Adelman) encryption scheme, widely used in the Internet, at banks and in secret services. Nevertheless, there is still no formal proof that Shor's algorithm outperforms any potential classical algorithm. This is different from the case of another quantum algorithm created by Lov Grover in 1997 [15], which shows a definite improvement over the classical case, although the speed-up is less impressive than for Shor's algorithm. Grover's algorithm is designed to perform a search in an unsorted database. The time required to find one desired element out of $N$ is proportional to $\sqrt{N}$, while in the classical case it is proportional to $N$. At the same time that the first quantum algorithms were proposed, the first quantum error correcting codes were developed. The possibility to implement error correcting codes encouraged researchers to work on physical implementations of quantum computers, since these codes relax the demands on control over noise and undesired interactions of the computer with the surrounding environment. Since the appearance of the first quantum algorithms, quantum computation has undergone a rapid development and growth, both from the theoretical and applied points of view. Many set-ups have been proposed for the hardware of a quantum computer [9, 16–19], arising from different fields of research including cold trapped atoms, nuclear magnetic resonance, Josephson junctions, and electrons in quantum dots, just to mention a few. The sort of physical attributes exploited in each case for the representation, storage and manipulation of information varies over a wide range.

Formally, a quantum computation is performed through a set of transformations, called *gates* [20]. A gate applies a unitary transformation $U$ to a set of qubits in a quantum state $|\Psi\rangle$. At the end of the calculation, a measurement is performed on the qubits (which are in the state $|\Psi'\rangle = U|\Psi\rangle$). There are many ways to choose sets of *universal* quantum gates. These are sets of gates from which any computation can be constructed, or at least approximated as precisely as desired. Such a set allows one to perform any arbitrary calculation without inventing a new gate each time. The implementation of a set of universal gates is therefore of crucial importance. It can be shown that it is possible to construct such a set with gates that act only on one or two qubits at a time [21].

The successful implementation of a quantum computer demands that some basic requirements be fulfilled. These are known as the DiVincenzo criteria [22] and can be summarized in the following way.

(i) *Information storage—the qubit.* We need to find some *quantum* property of a *scalable* physical system in which to encode our bit of information, that lives long enough to enable us to perform computations.

(ii) *Initial state preparation.* It should be possible to set the state of the qubits to zero before each new computation.

(iii) *Isolation.* The quantum nature of the qubits should be tenable; this will require enough isolation of the qubit from the environment to reduce the effects of decoherence.

(iv) *Gate implementation.* We need to be able to manipulate the states of individual qubits with reasonable precision, as well as to induce interactions between them in a controlled way, so that the implementation of gates is possible. Also, the gate operation time $\tau_s$ has to be much shorter than the decoherence time $T_2$, so that $\tau_s/T_2 \ll r$, where $r$ is the maximum tolerable error rate for quantum error correction schemes to be effective.

(v) *Readout.* It must be possible to measure the final state of our qubits once the computation is finished, to obtain the output of the computation.

To construct quantum computers of practical use, we emphasize that the *scalability* of the device should not be overlooked. This means it should be possible to enlarge the device to contain many qubits, while still adhering to all requirements described above. It should be mentioned here that this represents a challenging issue in most of the physical set-ups proposed so far. In this respect, very promising schemes for quantum computation are the proposals based on solid-state qubits [9, 17, 19, 23–30], which could take advantage of existing technology. In the following, we will concentrate on proposals based on solid-state qubits, describing them in more detail and summarizing recent achievements in the field.

## 2. Proposals for quantum computing

Before even the most rudimentary quantum circuits can be built, the elementary registers (qubits) and quantum gates must be designed. If any proposed design is to be considered for experiment, it should first be subjected to a battery of theoretical tests to ensure its feasibility in real physical situations. The five DiVincenzo criteria [22] (introduced in section 1) provide a simple checklist for the basic requirements of any physically realizable quantum computer. Demonstrating strong adherence to these criteria is a daunting task, which requires a broad understanding of material properties, physical phenomenology and the quantum mechanical time evolution of these systems. To make matters worse, a quantum computer, by *necessity*, must remain in a phase-coherent state far from thermodynamic equilibrium under conditions of strong time-dependent inter-qubit interactions (required for gating operations). These conditions are beyond the reach of much of the theoretical physicist's toolbox and therefore make the development of new proposals both a challenging and exciting endeavour.

The first proposals for quantum computing made use of cavity quantum electrodynamics (QED) [31], trapped ions [18], and nuclear magnetic resonance (NMR) [16]. All of these proposals benefit from potentially long decoherence times, relative to their respective gating times (however, see section 2.8 below for a discussion of the relative decoherence times in trapped ion systems that have been realized in experiment). In all three cases, this is due to a very weak coupling of the qubits to their environment. The long decoherence times for these proposals and existing experimental expertise led to quick success in achieving experimental realizations. A conditional phase gate was demonstrated early on in cavity QED systems [32]. The two-qubit controlled-NOT gate, which along with single-qubit rotations allows for universal quantum computation [21], has been realized in single-ion [33] and two-ion [34] versions. The most remarkable realization of the power of quantum computing to date is the implementation of Shor's algorithm [13] to factor the number 15 in a liquid-state NMR quantum computer [35]. In spite of their great successes, the proposals based on cavity QED, trapped ions and NMR may not satisfy the first DiVincenzo criterion. Specifically, these proposals may not meet the requirement that the quantum computer can be scaled up to contain a large number of qubits [9]. The requirement for scalability motivated the Loss–DiVincenzo proposal [9] for a solid-state quantum computer based on electron spin qubits. This proposal was quickly followed by a series of proposals for alternative solid-state realizations [19, 23, 24, 17, 25–30] and realizations for trapped atoms in optical lattices that may also be scalable [36, 37]. In the following sections we give a non-exhaustive survey of some of these proposals. The goal of this survey is to demonstrate how the various requirements for quantum computing have been met through example.

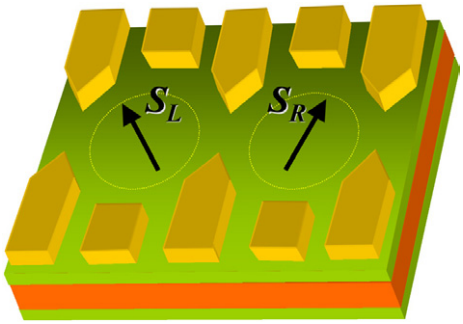


**Figure 1.** Two neighbouring electron spins confined to quantum dots, as in the Loss–DiVincenzo proposal. The lateral confinement is controlled by top gates. A time-dependent Heisenberg exchange coupling $J(t)$ can be pulsed high by pushing the electron spins closer, generating an appreciable overlap between the neighbouring orbital wavefunctions.

### 2.1. Quantum dot quantum computing

The qubits of the Loss–DiVincenzo quantum computer are formed from the two spin states $(|\uparrow\rangle, |\downarrow\rangle)$ of a confined electron. The considerations discussed in this proposal are generally applicable to electrons confined to any structure, such as atoms, molecules etc, although the original proposal focuses on electrons localized in quantum dots. These dots are typically generated from a two-dimensional electron gas (2DEG), in which the electrons are strongly confined in the vertical direction. Lateral confinement is provided by electrostatic top gates, which push the electrons into small localized regions of the 2DEG (see figures 1 and 2). Alternative quantum dot structures are discussed in section 4. Initialization of the quantum computer can be achieved by allowing all spins to reach their thermodynamic ground state at low temperature $T$ in an applied magnetic field $B$ (i.e., virtually all spins will be aligned if the condition $|g\mu_B B| \gg k_B T$ is satisfied, with $g$-factor $g$, Bohr magneton $\mu_B$, and Boltzmann's constant $k_B$). Several alternative initialization schemes have been investigated (see sections 4.5 and 4.9). Single-qubit operations can be performed, in principle, by changing the local effective Zeeman interaction at each dot individually. To do this may require large magnetic field gradients [38], $g$-factor engineering [39], magnetic layers (see figure 2), the inclusion of nearby ferromagnetic dots [9], polarized nuclear spins, or optical schemes (see section 5.2). In the Loss–DiVincenzo proposal, two-qubit operations are performed by pulsing the electrostatic barrier between neighbouring spins. When the barrier is high, the spins are decoupled. When the inter-dot barrier is pulsed low, an appreciable overlap develops between the two electron wavefunctions, resulting in

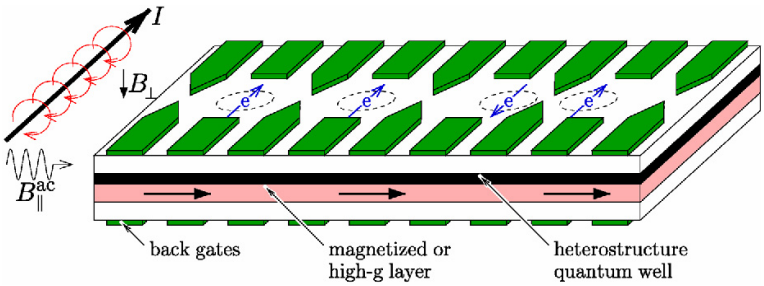


**Figure 2.** An array of exchange-coupled quantum dots. Top gates provide lateral confinement and allow pulsing of the exchange interaction for two-qubit operations (in this image the two dots on the left are decoupled, whereas the two dots on the right are coupled). Back gates could pull electrons down into a region of higher $g$-factor to allow single-qubit operations in conjunction with applied constant ($B_\perp$) and rf ($B_\parallel^{ac}$) magnetic fields.

a non-zero Heisenberg exchange coupling $J$. The Hamiltonian describing this time-dependent process is given by

$$H(t) = J(t)\mathbf{S}_L \cdot \mathbf{S}_R. \tag{1}$$

This Hamiltonian induces a unitary evolution given by the operator $U = \mathcal{T}\exp\{-i\int H(t)\,dt/\hbar\}$, where $\mathcal{T}$ is the time-ordering operator. If the exchange is pulsed on for a time $\tau_s$ such that $\int J(t)\,dt/\hbar = J_0\tau_s/\hbar = \pi$, the states of the two spins, with associated operators $\mathbf{S}_L$ and $\mathbf{S}_R$, as shown in figure 1, will be exchanged. This is the SWAP operation. Pulsing the exchange for the shorter time $\tau_s/2$ generates the 'square root of SWAP' operation, which can be used in conjunction with single-qubit operations to generate the controlled-NOT (quantum XOR) gate [9]. In addition to the timescale $\tau_s$, which gives the time to perform a two-qubit operation, there is a timescale associated with the rise/fall-time of the exchange $J(t)$. This is the switching time $\tau_{sw}$. When the relevant two-spin Hamiltonian takes the form of an ideal (isotropic) exchange, as given in (1), the total spin is conserved while switching. However, to avoid leakage to higher *orbital* states during gate operation, the exchange coupling must be switched adiabatically. More precisely, $\tau_{sw} \gg 1/\omega_0 \approx 10^{-12}$ s, where $\hbar\omega_0 \approx 1$ meV is the energy gap to the next orbital state [9, 40–42]. We stress that this timescale is valid only for the ideal case of a purely isotropic exchange interaction. When the exchange interaction is anisotropic, different spin states may mix and the relevant timescale for adiabatic switching may be significantly longer. For scalability, and application of quantum error correction procedures in *any* quantum computing proposal, it is important to turn off inter-qubit interactions in the idle state. In the Loss–DiVincenzo proposal, this is achieved with exponential accuracy since the overlap of neighbouring electron wavefunctions is exponentially suppressed with increasing separation. A detailed investigation of decoherence during gating due to a bosonic environment was performed in the original work of Loss and DiVincenzo. Since then, there have been many studies of leakage and decoherence in the context of the quantum dot quantum computing proposal. We discuss some of these studies in section 3, after reviewing alternative solid-state proposals for quantum computing.

### 2.2. Superconducting qubits

Among the first proposals for solid-state quantum computing were qubits based on superconducting Josephson junctions [43, 44, 23, 19, 45]. These proposals were quick to take advantage of the macroscopic quantum coherence afforded in such structures, and a large and well developed literature on their non-equilibrium dynamics [46]. The development of new designs for superconducting qubits has become an industry in itself. There are, for example, designs that exploit the d-wave pairing symmetry of cuprate high-temperature superconductors [47, 48] and Andreev bound states [49]. The observation of coherent oscillations in superconducting qubits [50, 51] was a watershed for the field of solid-state quantum information, demonstrating conclusively that quantum coherence could be generated and sustained for many precession periods ($\sim 10^4$ in the experiment by Vion *et al* [50]). More recent achievements of the superconducting proposals include the demonstration of a controlled-NOT gate [52] and the controlled coupling of a superconducting qubit to a single microwave photon mode [53]. In spite of these successes, the reduced visibility of coherent oscillations and the particular sources and nature of decoherence for these devices remain the subject of investigations [54–56]. Extensive reviews of Josephson-junction qubits can be found in [57, 58].

### 2.3. Quantum computing and the quantum Hall effect

Based on observed long lifetimes for nuclear spin states, Privman *et al* [24] have proposed a quantum computer composed of nuclear spins embedded in a two-dimensional electron gas (2DEG) in the quantum-Hall regime. The qubits of their proposal are encoded in the states of nuclear spins, which must be sufficiently separated to avoid dipolar coupling, but close enough ($\sim$10 nm) to allow significant interaction via the electron gas. Initialization of the qubits is achieved by placing spin-polarized conducting strips with a current of electrons above the nuclear spin qubits. The contact hyperfine interaction between electron and nuclear spins causes a polarization transfer from the electrons in the strips to the nuclear spins, preferentially orienting the nuclear spins along the electron spin polarization direction. Readout is performed in a complementary manner, with a transfer of polarization from the nuclear spins to electrons in the conducting strips. Single-qubit operations are performed via standard NMR pulses, which would require strong magnetic field gradients or many different nuclear spin species to bring single specific nuclear spins into resonance, while leaving the other qubits unchanged. A pairwise interaction between the nuclear spin qubits is necessary for the implementation of two-qubit gates. This interaction is generated by a superexchange,

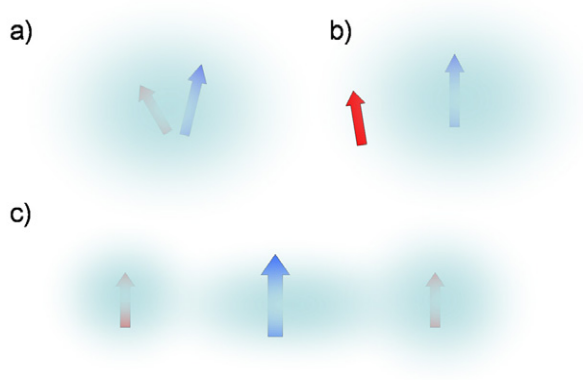


**Figure 3.** Schematic diagram illustrating the Fermi contact hyperfine interaction. Electron spins are represented by longer arrows and nuclear spins are represented by shorter arrows. The electron cloud is indicated with shading. (a) The direct exchange interaction is proportional to the electron density at the position of the nucleus. The interaction is strong when the electron is close. (b) The interaction is weaker when the nuclear spin is far from the centre of the electron wavefunction. (c) When two nuclear spins couple to the same (delocalized) electron, an effective exchange interaction between nuclear spins is generated.

mediated by electrons in the quantum Hall fluid that surrounds the nuclear spins (see figure 3(c)). The electron gas that couples the nuclear spins should be in the quantum Hall regime to avoid Friedel oscillations in the electron density, and hence a rapidly varying RKKY exchange [59, 60]. To perform computations, it is necessary to switch the interaction on and off. In the original work of Privman *et al* it was not clear how best to pulse the inter-qubit interaction [24]. Topics such as switching error (leakage to states outside the qubit basis) and perhaps the most important of all, decoherence, are not addressed in the original work of Privman *et al*. However, subsequent studies of the decoherence of nuclear spins in the integer quantum Hall regime have led to the prediction that the decoherence time for these qubits could be as long as $T_2 \simeq 10^{-1}$ s [60, 61].

### 2.4. Shallow-donor quantum computing

Following the proposals of Loss–DiVincenzo and Privman *et al*, Kane [17] has introduced a proposal that takes advantage of the long lifetimes of nuclear spins (as in the proposal of Privman *et al*) and electrically controlled gating of two-qubit interactions (as in the Loss–DiVincenzo proposal). This proposal uses the nuclear spins of $^{31}$P donor impurities in silicon as its qubits. Each donor impurity is associated with a weakly bound electron in an s-type orbital state. One- and two-qubit operations are performed with electrostatic '$A$-gates' and '$J$-gates', respectively. These gates take their names from the conventional symbols for the contact hyperfine ($A$) and spin exchange ($J$) coupling constants. The $A$-gates adjust the position of the electron cloud relative to the donor nucleus (see figures 3(a), (b)). In this way, the magnitude of the contact hyperfine interaction is varied, bringing the nuclear spins in and out of resonance with a uniform applied magnetic field. Two-qubit operations are performed via an electron-mediated superexchange between neighbouring nuclear-spin qubits (figure 3(c)), as in the proposal of Privman *et al*. The $J$-gates adjust the overlap of electron clouds on neighbouring impurities, thus controlling the strength of the superexchange. Readout of the qubits is performed by transferring nuclear spin information back to the electron spins and observing the resulting orbital electron wavefunction via standard capacitive techniques. The original work of Kane includes a discussion of decoherence due to a fluctuating gate voltage. This work does not, however, discuss the influence of the nuclear dipole–dipole interaction [62], problems associated with a violently position-dependent exchange interaction [63], or decoherence mechanisms that could affect the electron spin during gate operation or measurement. These mechanisms include spin–orbit coupling and the contact hyperfine interaction with surrounding nuclear spins.

### 2.5. Spin-cluster qubits

With the exception of proposals such as the 'exchange-only' scheme [64], nearly all quantum computing architectures require single-qubit operations. Addressing single spin qubits with magnetic resonance pulses usually requires magnetic field gradients or $g$-factor engineering to bring the spins into resonance individually. To implement two-qubit gates, the spin qubits must typically be separated by very small distances (on the order of the electron wavefunction: $\simeq$50 nm in quantum dots, $\simeq$10 nm in the proposal of Privman *et al*, and $\simeq$5 nm for an electron bound to a phosphorus donor in silicon). This requirement leads to extremely large magnetic field or $g$-factor gradients, which may not be practical in a typical laboratory setting. To resolve this issue, Meier *et al* [26] have proposed a scheme for quantum computing based on antiferromagnetic spin clusters, rather than single spins. In this proposal the quantum computer consists of many spin clusters. Each cluster contains an odd number of antiferromagnetically exchange-coupled spins. The two basis states of the qubit are encoded in the ground-state doublet formed by two total-$S_z$ eigenstates for one cluster. Since its basis corresponds to two total spin-$S_z$ eigenstates with an associated magnetic moment, the qubit can be manipulated with a magnetic field to perform single-qubit operations in the same way as for a single spin 1/2. Furthermore, the qubit basis is protected from higher-lying states by a gap of order $\Delta \sim J\pi^2/2n_c$ for a cluster containing $n_c$ spins with exchange coupling $J$ [26]. To perform two-qubit operations, separate clusters are coupled at their ends by a tunable exchange. Initialization of the qubits is achieved by cooling the system to its ground state in a strong magnetic field, as in the Loss–DiVincenzo proposal. Since the two orthogonal states of the ground-state doublet resemble classical Néel ordering with the magnetization alternating $\uparrow\downarrow\uparrow\ldots$, or $\downarrow\uparrow\downarrow\ldots$, readout can be performed, in principle, with a local magnetization measurement. Decoherence due to magnetic field fluctuations has been considered in this work. There is no increase in the decoherence rate (over the single-spin rate) for a magnetic field that fluctuates uniformly over the cluster, although there is a linear increase with cluster size for local magnetic fields that fluctuate independently.

### 2.6. Quantum computing with molecular magnets

Recently there has been significant interest in using molecular magnets for quantum computing applications. These systems

exhibit a number of interesting quantum mechanical features that can be probed in experiment, including quantum tunnelling [65], interference effects [66], and the coherent superposition of high-spin states [67] (for a review, see [68]). Additionally, molecular magnets can be well understood in terms of relatively simple spin Hamiltonians, which means that high-resolution spin resonance spectroscopy [69] or specific heat measurements [70] can be used to extract the relevant coupling constants empirically.

Leuenberger and Loss [71] have introduced a proposal to perform Grover's algorithm in ensembles of large-spin molecular magnets. Since this proposal relies only on a well defined multilevel quantum system with non-equidistant level spacing, the same procedure can be applied to nuclear spins in GaAs in the presence of the nuclear quadrupole interaction [72, 73] or to multilevel Josephson junction devices, where coherent oscillations have now been observed [74]. We note that Grover's algorithm has been implemented experimentally using atomic Rydberg states [75]. While these proposals and experiments are valuable for demonstrating the practical implementation of quantum computation, they rely on single multilevel systems, and are therefore not scalable. Finally, the very recent proposal of Troiani *et al* [70, 76] suggests using the molecular magnet $Cr_7Ni$ as a real-world implementation of the spin-cluster quantum computing scheme discussed in the previous section.

### 2.7. Silicon valley

For quantum computing and spintronics applications, silicon has advantages over other semiconductors. First, silicon has long been a staple for the electronics industry. Second, the spin–orbit interaction in silicon is weak (evidence of this is provided by the small difference in effective electron-spin $g$-factor from the free value). Third, natural silicon contains only 4.7% nuclear-spin-carrying isotopes, which significantly reduces the effects of the contact hyperfine interaction relative to materials such as (Ga/In)As. Silicon quantum dots are, however, not as advanced as the alternatives made from III–V semiconductors, and silicon is an indirect gap semiconductor (in contrast to the direct gap material GaAs), which limits its use in optical applications. Nevertheless, silicon's prevalence in industry means that purification and fabrication techniques are usually better established than for other semiconductors.

Levy [27] has suggested specializing the Loss–DiVincenzo proposal to Ge/Si quantum dots. Instead of using top gates to confine electron spins laterally, these dots would be defined by patterning a ferroelectric material (which has a finite electric dipole moment) on the surface of a 2DEG. In this proposal, two-qubit gating operations would be performed by applying optical excitation to the ferroelectric, which changes the local electric field that defines neighbouring quantum dots. This change in the local electrostatic potential generates a pulsed exchange interaction between neighbouring electron spins. The electrical pulsing, which defines the rise-time (switching time) $\tau_{sw}$ for the exchange coupling, occurs at terahertz frequencies ($\tau_{sw} \approx 10^{-12}$ s). This short timescale will likely violate the adiabaticity criterion discussed in section 2.1. To satisfy the adiabaticity criterion, Levy suggests using a third dot to mediate a superexchange between qubit dots, as in [77].

Ladd *et al* [28, 78] have proposed an all-silicon quantum computer, where the qubits are generated from $^{29}$Si nuclear spins embedded in a $^{28}$Si matrix. In a sufficiently large magnetic field gradient, provided by a strong Dy ferromagnet, single-qubit operations could be performed with NMR pulses and two-qubit operations could be performed by pulsing the dipole–dipole interaction between neighbouring nuclear spins (which would be suppressed in the idle state with an appropriate sequence of NMR averaging pulses). Readout in this proposal would be provided by magnetic resonance force microscopy (MRFM) [79, 80], where the nuclear spin state couples to vibrational modes of a cantilever or thin silicon bridge. Recent success in the detection of the *existence* of a single electron spin with MRFM is very promising, although it has not yet been shown experimentally that a single-spin quantum *state* can be measured using this technique [81] (see also section 4.6 below for a description of MRFM detection).

The recent proposal of Friesen *et al* [29] uses electron spins confined to silicon quantum dots. This proposal is based on the Loss–DiVincenzo quantum dot quantum computer, specialized to a silicon environment. Friesen *et al* have developed a strategy for initialization and readout via spin-charge conversion, which has been modelled in detail in [82]. Two-qubit operations are performed, as in the original Loss–DiVincenzo proposal, by pulsing a direct exchange between neighbouring electrons using electrostatic gates to increase or decrease the overlap between neighbouring electron wavefunctions. Friesen *et al* have performed a detailed calculation of exchange versus gate voltages to find the correct operating regime for their proposed quantum computer. In addition, they consider decoherence due to fluctuations in gate voltage, but do not address other channels of decoherence.

Perhaps one of the most challenging quantum computing proposals comes from Stoneham *et al* [30, 83, 84]. The qubits of their proposal consist of electron spins bound to deep-donor impurities in silicon. Between each pair of qubits, there is a control atom. By optically exciting an electron from the highest valence state of the control atom to a molecular state formed between the deep donors, a superexchange is generated between neighbouring qubits, which can be turned off again by stimulated de-excitation. The qubits in this proposal are addressed individually by using 'site selectivity' (every qubit has a unique environment, therefore a unique energy-level structure). Since the energies involved in the gating process are large, Stoneham *et al* suggest that this proposal could potentially operate at room temperature.

### 2.8. Hybrid proposals

In an attempt to extract the best from both worlds, there have been proposals for hybrid quantum computers. These proposals aim to couple ideas from proven approaches to quantum computing (cavity QED, trapped ions and trapped atoms) with the benefits offered by solid-state implementations.

Imamoğlu *et al* [25] have suggested a scheme that combines cavity QED and spin-based quantum dot quantum computing. The qubits of this proposal are encoded in the spin states of quantum dots, as in the Loss–DiVincenzo proposal. The quantum dots are contained within a semiconductor

microcavity, with well defined optical modes. Single-qubit operations are performed by addressing individual dots with optical fibres and coupling the spin-up and spin-down states via a Raman process, induced by laser excitation. To perform two-qubit operations, distant electron spins are coupled via a delocalized cavity mode. This induces an XY-like interaction between electron spins. In the original work of Imamoğlu *et al*, it was shown that an XY-interaction and single-qubit rotations are sufficient to perform a two-qubit CNOT-gate. Single-spin readout could be performed in this proposal by exciting a spin-selective transition in which a photon is emitted (or not emitted) depending on the electron spin state. In this way, the state of the single electron spin is determined by the presence or absence of a single photon.

Quantum optical proposals and implementations often use the hyperfine (spin) and vibrational states of trapped ions and atoms as their qubits. The coupling strengths for these states are typically very small relative to their solid-state counterparts. This means that decoherence times ($T_2$) for these implementations are relatively long (for example, $T_2 \simeq 170\ \mu$s in [85]). For the same reason, however, the relevant gating times ($\tau_s$) are also relatively long ($\tau_s \simeq 10\ \mu$s for a CNOT gate in [85]). The ratio of gating to decoherence time that has been observed $r = \tau_s/T_2 \approx 1/17$ greatly exceeds current estimates for the error threshold allowable for effective quantum error correction. To remedy this potential difficulty, a very recent proposal by Tian *et al* [86] suggests a combined quantum optical and solid-state device. In this proposal the states of trapped atoms or ions would be used as a long-lived quantum information storage device during the idle state. When fast one- or two-qubit operations are to be performed, information is transferred to some solid-state device (electron spins in quantum dots or superconducting qubits) then returned again to the storage device when the operation is complete.

## 3. Obstacles to quantum dot quantum computing

Several major obstacles to quantum dot quantum computation were identified and addressed in the original work of Loss and DiVincenzo [9], and later elaborated upon [87, 88, 1]. These obstacles include entanglement (the creation and transport of a coherent superposition of states), gating error (leakage to higher states outside the qubit basis during gate operation), and perhaps most importantly coherence (the preservation of any given superposition in the presence of a coupling to the environment). In the rest of this section we review work that has been done to understand and possibly surmount these three obstacles in the context of the Loss–DiVincenzo proposal.

### *3.1. Flying qubits and entanglement generation*

In addition to the five DiVincenzo criteria for quantum *computation* introduced in section 1, there are two 'desiderata', which are important for performing quantum *communication* tasks. These desiderata, which were addressed in [87], are summarized in the following statements [22].

(vi) The ability to inter-convert stationary and flying qubits.
(vii) The ability to faithfully transmit flying qubits between distant locations.

The whimsical term 'flying qubits' refers to qubits that can be conveniently moved from place to place. The most obvious (and common) choice for a flying qubit is provided by the polarization states of photons [32]. In the context of quantum dot quantum computing, this has led to a number of proposals for the conversion of quantum information [25, 89–92] or entanglement [93] from spin to light, and *vice versa*. More recent work has suggested that 'free electron quantum computation' may be possible in principle [94, 95], in which mobile electrons (in some material) travelling between dots could replace photons as the flying qubit medium of choice.

Deeply connected to the implementation of flying qubits is the creation of nonlocal entanglement. The race to create and measure [87, 96–100] entangled particle pairs has led to a virtual industry of so-called 'entangler' proposals for the spin [87, 96, 239, 101–112] and orbital [113–115] degrees of freedom. These proposals have the very ambitious goal of generating and spatially separating a many-particle quantum superposition that cannot be factorized into single-particle states. The canonical example of such a state for the spin degree of freedom is the singlet formed from two spin-1/2 particles: $(|\uparrow\downarrow\rangle - |\downarrow\uparrow\rangle)/\sqrt{2}$. The various efforts related to spin entanglement include proposals to extract and separate spin-singlet pairs from a superconductor through two quantum dots [101] or Luttinger-liquid leads [107, 108] and proposals that generate entanglement near a magnetic impurity [104], through a single dot [105], from biexcitons in double quantum dots [89], through a triple dot [109], and from Coulomb scattering in a two-dimensional electron gas [112]. Entanglement generation and measurement remains a lofty goal for those working on solid-state quantum computing, theorists and experimentalists alike. Recent experiments [116] that have measured the concurrence (an entanglement measure) for electrons in the ground state of a two-electron quantum dot point to a promising future for entanglement-related phenomena in the solid state (see also section 5.3). For recent reviews on entanglement generation and measurement, see [117, 118].

### *3.2. Gating error*

Hu and Das Sarma have evaluated the probability for double occupancy of one of the dots in the Loss–DiVincenzo proposal using Hartree–Fock and molecular orbital techniques [119]. They suggest that it may be difficult to achieve both a significant exchange coupling and low double-occupancy probability. Schliemann *et al* [40, 41] and more recently Requist *et al* [42] have investigated the probability for double-occupancy gating errors in a pair of coupled quantum dots during SWAP gate operation. Through numerical and analytical study they have found that the Loss–DiVincenzo proposal is very robust against double-occupancy errors when operated in the adiabatic regime (defined in section 2.1). Barrett and Barnes [120] have subsequently shown that *orbital* dephasing can result in a significant error rate ($10^{-2}$–$10^{-3}$ errors per gate operation). This is comparable to current estimates for the maximum error rate allowable for quantum error correction to be effective [121], but further studies on the nature of the spin–orbit interaction have suggested that the spin–orbit coupling can be minimized with careful pulsing of

**Table 1.** Relevant energy scales for the Loss–DiVincenzo quantum computing proposal. The above estimates are based on a GaAs dot of lateral size $l = 30$ nm containing $N = 10^5$ nuclear spins. The typical size-quantization energy $\hbar\omega_0$ and exchange coupling $J$ for a dot of this size are taken from [88]. The Rashba ($\alpha$) and Dresselhaus ($\beta$) coefficients were extracted from experimental data in [125]. The hyperfine interaction constant $A$ was estimated from a weighted average over the hyperfine coupling constants for the three nuclear spin species in GaAs in [126]. The nuclear spin dipolar coupling is estimated from the linewidth of the NMR resonance in [126], which gives a correlation time $\tau_{dd} \approx 10^{-4}$ s.

| | Symbol | Description | Estimate (meV) | References |
|---|---|---|---|---|
| 1 | $\hbar\omega_0$ | Size-quantization energy | 1 | [88] |
| 2 | $J$ | Electron spin exchange coupling | $10^{-1}$ | [88] |
| 3 | $\hbar \max\{\|\alpha\|, \|\beta\|\}/l$ | Spin–orbit coupling strength | $10^{-2}$ | [125] |
| 4 | $A$ | Hyperfine interaction (polarized nuclei) | $10^{-1}$ | [126] |
| 5 | $A/\sqrt{N}$ | Hyperfine interaction (unpolarized nuclei) | $10^{-4}$ | — |
| 6 | $A/N$ | Knight shift dispersion | $10^{-6}$ | — |
| 7 | $N\mu_B\mu_N/l^3$ | Electron–nuclear dipolar coupling | $10^{-7}$ | — |
| 8 | $\hbar/\tau_{dd}$ | Nuclear–nuclear dipolar coupling | $10^{-8}$ | [126] |
| 9 | $\mu_B^2/l^3$ | Electron–electron dipolar coupling | $10^{-9}$ | — |

the exchange during gate operations (see section 3.3.1). When the potential barrier between quantum dots is pulsed low, the overlap between nearest-neighbour dots is appreciable, while that between next-nearest and next-next-nearest neighbours is exponentially suppressed with distance. In spite of the smallness of these interactions, Mizel and Lidar [122] have recently suggested that three- and four-spin interactions in a realistic quantum computing proposal may lead to substantial gating errors. These problems are, however, specific to a particular architecture, and it is possible that they could be corrected or exploited by adjusting the device design [122].

### 3.3. Decoherence

Every experimental apparatus shows some small fluctuations in electrostatic voltage and applied magnetic field. These fluctuations, acting on an electron spin in a quantum dot, will inevitably induce decay of the spin directly through the Zeeman interaction (in the case of a fluctuating magnetic field), or indirectly through spin–orbit coupling (in the case of a fluctuating electric field). The effect of these fluctuations can be treated accurately (for a weak coupling to the electron spin) by the phenomenological spin-boson model within a Born–Markov approximation, as derived in [9]. The coupling of the electron spin to the bath cannot always be treated as weak, and effects of the bath memory (non-Markovian evolution) may be important for achieving the level of accuracy required to perform quantum error correction. For these reasons, the solution to this model has recently been extended to obtain non-Markovian effects [123] and corrections beyond the Born approximation [124] in the case of ohmic dissipation in the bath.

Fluctuations in voltage and magnetic field are artifacts of a given experimental apparatus. In principle, these fluctuations can be reduced with improved electronics, and can therefore be regarded as *extrinsic* sources of decoherence. In addition to these extrinsic sources, there are sources of decoherence that are *intrinsic* to the quantum dot qubit design. These include the coupling of the electronic spin to phonons in the surrounding lattice or other fluctuations via the spin–orbit interaction [127, 88, 128–133] and coupling of the electron spin to surrounding nuclear spins via the contact hyperfine interaction [88, 134–148]. A detailed understanding of the electron spin evolution under the influence of these interactions is of fundamental interest and is necessary to implement reliable quantum dot quantum computation. The first step to understanding any decoherence mechanism is to estimate its size. In table 1 we give estimates for various energy scales related to decoherence and qubit operation in the Loss–DiVincenzo proposal.

*3.3.1. Spin–orbit coupling.* We would like to assess the spin–orbit coupling strength for typical quantum dots. Performing the standard non-relativistic expansion and reduction to a two-component spinor for a Dirac electron to leading order in $1/mc^2$ leads to the spin–orbit coupling term [149]

$$H_{so} = \frac{\hbar}{2m^2c^2}(\nabla V(\mathbf{r}) \times \mathbf{P}) \cdot \mathbf{S}. \tag{2}$$

In the above, $m$ is the electron mass, $c$ is the speed of light, $V(\mathbf{r})$ is the potential experienced by the electron, $\mathbf{P}$ is the momentum operator in three dimensions, and $\mathbf{S}$ is the electron spin-1/2 operator. For a spherically symmetric parabolic confining potential, $V(\mathbf{r}) = m\omega_0^2 r^2/2$, the spin–orbit coupling term is $H_{so} = (\omega_0^2/2mc^2)\mathbf{L} \cdot \mathbf{S}$. Here, $\mathbf{L} = \mathbf{r} \times \mathbf{P}$ is the orbital angular momentum operator, which can be substituted with $\hbar$ for estimation purposes. Comparing the strength of this coupling to the orbital energy $\hbar\omega_0 \approx 1$ meV gives $\langle H_{so}\rangle/\hbar\omega_0 \approx 10^{-7}$ [127, 88]. This smallness of the spin–orbit coupling compared to the orbital energy scale would suggest that the electron spin in quantum dots is relatively free from external influences that couple to its charge. In realistic dots, however, the confining potential is neither smooth (it has a $1/r$ singularity at the centre of each lattice ion) nor spherically symmetric, and the resulting spin–orbit interaction takes on a more complicated form. In a crystalline solid, the spin–orbit interaction is the sum of structure inversion asymmetry (Rashba) [150] and bulk inversion asymmetry (Dresselhaus) [151] terms, which can be written for an electron confined to two dimensions as

$$H_{so} = \alpha(p_x\sigma_y - p_y\sigma_x) + \beta(-p_x\sigma_x + p_y\sigma_y) + O(|\mathbf{p}|^3). \tag{3}$$

$\alpha$ ($\beta$) is the Rashba (Dresselhaus) coefficient, $\mathbf{p} = (p_x, p_y)$ is the electron momentum operator in the $x$–$y$ plane, and

$\sigma_{x,y}$ are the usual Pauli matrices. For a strongly two-dimensional system, the cubic Dresselhaus term, of order $\sim|\mathbf{p}|^3$, can be neglected relative to the Rashba and linear Dresselhaus terms, which have the size $\sim p_{x,y}p_z^2$ [152]. In a two-dimensional quantum dot, we replace $p_z \approx \hbar/d$, $p_{x,y} \approx \hbar/l$, where $d$ is the 2DEG thickness and $l$ is the lateral quantum dot size. The cubic term is then smaller than the linear Dresselhaus and Rashba terms by a factor of order $\sim(d/l)^2$. The Rashba and Dresselhaus coefficients have been extracted from magnetoresistance data in a GaAs/AlGaAs 2DEG. This gives the values $\hbar\beta = (4 \pm 1)$ meV Å and $\hbar\alpha = (-5 \pm 1)$ meV Å [125]. To estimate the size of $H_{\rm so}$ given in (3) for a quantum dot containing a single electron, we replace the momenta by $p_{x,y} \approx \hbar/l$, where $l = 10$–$100$ nm. This gives the range $\langle H_{\rm so}\rangle = 10^{-2}$–$10^{-1}$ meV. This estimate is significantly larger than the value ($\simeq 10^{-7}$ meV) for a simple parabolic confining potential. All is not lost, however, since the spin–orbit coupling can only affect the spin *indirectly* through fluctuations in the orbital degree of freedom. We can only assess the real danger of this interaction through a correct microscopic analysis of the spin–orbit Hamiltonian in the proper context.

The direct effects that a realistic spin–orbit interaction has on two-qubit gating operations in a quantum computer have been explored by several authors. Bonesteel *et al* [153] have shown that the effect of the spin–orbit interaction on coupled quantum dot qubits can be minimized by using time-symmetric qubit gating. Subsequently, Burkard and Loss [154] have shown that the spin–orbit effect during gating can be eliminated completely for appropriately chosen exchange pulse shapes (see also [155]). Additionally, there have been several investigations into the possible spin-flip (relaxation) [128–132] and decoherence [156, 133] mechanisms mediated by the spin–orbit interaction and coupling to lattice phonons or other fluctuations. In many ways, an electron in the orbital ground state of a quantum dot is very similar to an electron bound to a donor impurity site. Since the spin relaxation and decoherence times for electrons bound to shallow donors were investigated many years ago [157, 158], much of this work has been used to accelerate progress for the analogous quantum dot structures.

Khaetskii and Nazarov have calculated the rates for spin-flip transitions due to the spin–orbit interaction both through direct relaxation from an excited orbital state accompanied by a spin flip [128], and through a virtual process between the two states of a Zeeman-split doublet within the same orbital state [129]. The most effective spin-flip mechanism for a transition between Zeeman-split states, which has a rate $1/T_1 \propto (g\mu_{\rm B}B)^5/(\hbar\omega_0)^4$, is significantly reduced for decreasing magnetic field $B$ and increasing orbital energy $\hbar\omega_0$.

In the presence of spin–orbit coupling, a precessing spin induces an oscillating electric field. Levitov and Rashba [130] have suggested that this coupling may be a double-edged sword in view of applications to spintronics. On the positive side, the time-varying electric field might provide access to the dynamics of a single isolated spin. The reverse mechanism, however, leads to a further channel for spin relaxation from excitations in the dot leads.

There have been further studies of spin–lattice relaxation mechanisms that are specialized to particular quantum dot architectures. Glavin and Kim [131] have compared results for Si quantum dots and donor impurities, and Cheng *et al* [132] have performed a numerical exact-diagonalization study for GaAs quantum dots, extending the validity of previous calculations to a more realistic set of wavefunctions.

The spin-flip (relaxation) time $T_1$ is important for applications of spintronics involving classical information, encoded in the states $|\uparrow\rangle$ and $|\downarrow\rangle$. However, for quantum computing tasks, the relevant timescale is the spin decoherence time $T_2$, which is the lifetime for a coherent superposition $a|\uparrow\rangle + b|\downarrow\rangle$. Typically, the decoherence time is much less than the relaxation time ($T_2 \ll T_1$). Golovach *et al* have shown that the fluctuations induced from spin–orbit coupling are purely transverse to the direction of an applied magnetic field to leading order in the coupling [133]. Because the fluctuations are purely transverse, the corresponding $T_2$ time due to the combined spin–orbit and electron–phonon interactions *exceeds* the value of the longitudinal spin relaxation time, giving $T_2 = 2T_1$. Moreover, for phonons in three dimensions, the spectral function is super-ohmic ($\sim\omega^3$) and thus the pure dephasing contribution is absent, again ensuring that $T_2 = 2T_1$. Provided other decoherence mechanisms can be arbitrarily suppressed, this result is very promising for applications of quantum dot quantum computing in view of recent experiments that show exceptionally long $T_1$ times for single electron spins confined to GaAs quantum dots (see section 4.3).

*3.3.2. Spin–spin coupling.* Unfortunately, the spin–orbit interaction is not the end of the decoherence story. The electron spin can also couple directly to other spins embedded in the quantum computer device. In a GaAs quantum dot, the electron wavefunction contains approximately $N = 10^5$ lattice nuclei, and every nucleus carries spin $I = 3/2$. The dominant spin–spin coupling for this type of dot arises from the Fermi contact hyperfine interaction. The Fermi contact hyperfine interaction for an electron with orbital envelope wavefunction $\psi(\mathbf{r})$ and spin operator $\mathbf{S}$ interacting with surrounding nuclear spins $I_k$ is described by the spin Hamiltonian

$$H_{\rm hf} = \sum_k A_k \mathbf{S}\cdot\mathbf{I}_k; \qquad A_k = v_0 A|\psi(\mathbf{r}_k)|^2. \tag{4}$$

Here, $v_0$ is the volume of a crystal unit cell containing one nuclear spin. Due to $H_{\rm hf}$, the electron spin will experience an effective magnetic field (the *Overhauser field*), which gives rise to an energy splitting on the order of $pIA$, where $I$ is the total nuclear spin and $p$ is the nuclear spin polarization. For full polarization of the nuclear spin system, the Overhauser field induces a splitting $\approx IA = 10^{-1}$ meV in GaAs. In a typical unpolarized sample, we have $|p| \approx 1/\sqrt{N}$, which gives a splitting $IA/\sqrt{N} \approx 10^{-4}$ meV for a quantum dot containing $N = 10^5$ nuclear spins. In addition, the nuclear spin at site $k$ will experience an effective Zeeman splitting (*Knight shift*) on the order of $A_k$. Since the coupling constants $A_k$ vary in space from $A_k \approx A/N = 10^{-6}$ meV near the dot centre to $A_k = 0$ far from the dot, nuclear spins at different sites will precess with different frequencies. This dispersion in the Knight shift will efficiently destroy collective states generated in the nuclear spin system on a timescale $t \approx \hbar N/A \approx 1$ $\mu$s [159], and is therefore important for proposals based on nuclear spin quantum computing.

In addition to the Fermi *contact* hyperfine term, there is an *anisotropic* contribution to the hyperfine interaction. For a widely separated electron and nucleus, the anisotropic hyperfine interaction reduces to the interaction energy between point dipoles:

$$H_{\rm dd} = \sum_k \frac{(g\mu_{\rm B})(g_I\mu_{\rm N})}{r^3}\left\{\frac{3(\mathbf{I}_k\cdot\mathbf{r})(\mathbf{S}\cdot\mathbf{r})}{r^2} - \mathbf{I}_k\cdot\mathbf{S}\right\}. \quad (5)$$

For a microscopic derivation of $H_{\rm hf}$ and $H_{\rm dd}$, see [160]. If the electron spin is in a spherically symmetric orbital s state with the nuclear spin at its centre, the anisotropic hyperfine interaction vanishes identically [160]. The contribution of this term from nuclear spins near the dot centre will therefore be small, but for nuclear spins near the edge of the electron wavefunction, which do not 'see' a spherical electron spin distribution, it may become appreciable. Assuming approximately $N = 10^5$ nuclear spins have a significant dipolar coupling to the electron, we estimate the size of the electron–nuclear dipolar interaction as $\langle H_{\rm dd}\rangle \approx N\mu_{\rm N}\mu_{\rm B}/l^3 \simeq 10^{-7}$ meV, where $l = 30$ nm is the typical dot size.

The final spin–spin coupling directly associated with the electron is the magnetic dipolar coupling of the electron to other electron spins in neighbouring quantum dots. This can be estimated as $\mu_{\rm B}^2/l^3 \approx 10^{-9}$ meV. Although this coupling is very weak for neighbouring single-electron quantum dots, it can become significant at atomic length scales, and may be a significant source of decoherence for other solid-state proposals [26]. In addition to direct electron spin coupling mechanisms, there are also significant mechanisms that couple the environment to itself. For example, the nuclear spins experience a mutual dipolar coupling. This dipolar coupling causes the nuclear environment to evolve dynamically, which can, in turn, affect the electron through direct hyperfine coupling. The nuclear spins evolve on a timescale given by the dipolar correlation time $\tau_{\rm dd} = 10^{-4}$ s. The time $\tau_{\rm dd}$ is determined from the linewidth of the NMR resonance (in bulk) through $\hbar/\tau_{\rm dd} \simeq 10^{-8}$ meV [126].

There have been many studies of electron spin dynamics in the presence of the strongest (Fermi contact hyperfine) spin–spin interaction. Burkard *et al* [88] showed that in the presence of the hyperfine interaction with surrounding nuclear spins, the electron spin-flip transition probability could be suppressed by applying a magnetic field $B$ or polarizing the nuclear spin system (this probability is suppressed by the factor $1/p^2N$ for $B = 0$, nuclear spin polarization $p$ and $N$ nuclear spins within the quantum dot). Erlingsson *et al* have investigated singlet–triplet transitions mediated by the contact hyperfine interaction [134] and transitions between a Zeeman-split doublet [135]. In an investigation of decoherence, Khaetskii *et al* [136, 137] have found an exact solution for the electron spin evolution under the action of $H_{\rm hf}$ in the particular case of a fully polarized nuclear spin system. They found that only a small fraction ($\simeq 1/N$) of the electron spin underwent decay and the resulting dynamics were described by a power-law or inverse logarithmic decay at long times. Schliemann *et al* [138] have performed exact diagonalizations on small nuclear spin systems. These exact diagonalization studies show that the hyperfine interaction can be very efficient in causing decay of the electron spin in small systems and that the dynamics of an ensemble are reproduced by the dynamics of a randomly correlated initial nuclear spin state. Yuzbashyan *et al* [148] have recently found an exact closed-form solution for the classical (mean-field) analogue of this problem and highlighted its connection to the dynamics of the BCS pairing model.

The gating operations performed on a quantum computer are performed on *single* isolated systems. This raises the question of whether ensemble or pure-state initial conditions should be used when calculating spin dynamics for the purpose of quantum computing. The free-induction decay of the electron spin in the presence of an ensemble of nuclear spin configurations has been investigated by Merkulov *et al* [139], who found a rapid initial Gaussian decay of the electron spin with a timescale $\tau \approx 1$ ns in GaAs. Even for a *single* quantum mechanical initial state of the nuclear system, the electron-spin free-induction decay can be severe. For a translationally invariant direct-product nuclear spin state with polarization $p$, and in the limit of a large number $N \gg 1$ of nuclear spins $I = 1/2$, and large magnetic field $|g\mu_{\rm B}B| \gg A$, the transverse electron spin $\langle S_+\rangle_t = \langle S_x\rangle_t + {\rm i}\langle S_y\rangle_t$ decays like a Gaussian [144] (up to a time-dependent phase factor):

$$\langle S_+\rangle_t \propto \langle S_+\rangle_0 \exp\left(-\frac{t^2}{2\tau_{\rm c}^2}\right); \qquad \tau_{\rm c} = \sqrt{\frac{N}{1-p^2}}\frac{2\hbar}{A}. \quad (6)$$

In GaAs, and for polarization $p \approx 0$, we have $\tau_{\rm c} \approx 5$ ns. The timescale $\tau_{\rm c}$ can be moderately extended by polarizing the nuclear spin system. However, even a polarization degree of 99% (the current record in a GaAs quantum dot is 60% [161], and significant gate-controlled nuclear spin polarization has been seen in a GaAs 2DEG in the quantum Hall regime [162]) would only extend the decay time by a factor of 10. If the state of the nuclear spins could be prepared, e.g., via a measurement, in an eigenstate of the total $z$-component of the nuclear Overhauser field, the decay in (6) would be removed. Under these conditions, the electron spin still undergoes a nontrivial non-Markovian (history dependent) dynamics on a timescale given by the inverse Knight shift dispersion $\hbar N/A \approx 1$ $\mu$s. This decay can be evaluated in the presence of a sufficiently large magnetic field [144].

An alternative way to remove the effects of the decay in (6) is to perform a spin-echo sequence on the electron [144]. The decay of the Hahn spin-echo envelope due to spectral diffusion (which includes the effect of the nuclear dipole–dipole interaction) has been investigated by de Sousa *et al* [140, 141] for a model with fluctuating classical nuclear spins $I = 1/2$, that evolve in a Markovian fashion. This same model has recently been extended to larger nuclear spin $I > 1/2$ [145].

In addition to work on the time-dependent evolution of a localized electron spin, there have been proposals for spintronic devices that use the contact hyperfine interaction to their advantage. These include a proposal for dynamic polarization of nuclear spins via optical manipulation of localized electrons [163] and a proposal for a nuclear spin quantum memory [164–166] that takes advantage of potentially long-lived nuclear states. The quantum memory proposal is limited by the Knight shift dispersion in quantum dots in the presence of an electron spin [159]. The electron

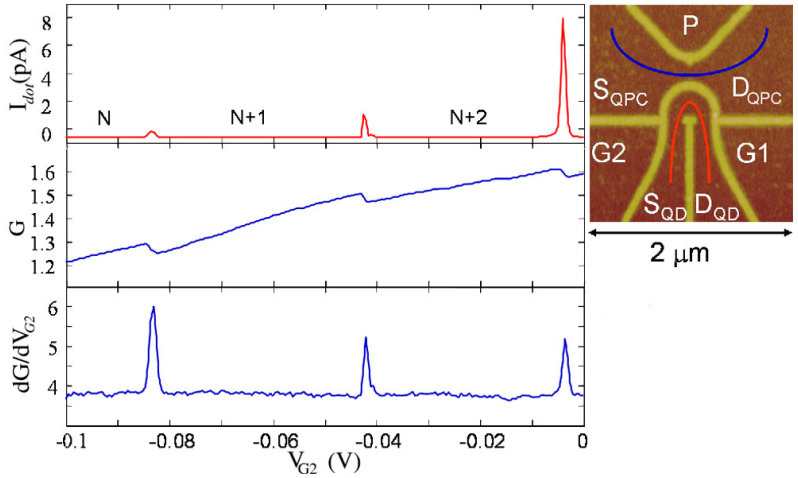


**Figure 4.** Device (right) used to read out the charge state of a quantum dot with a quantum point contact (QPC) from [167]. The plunger gate ($P$) controls the restriction of the QPC. $S_{QPC}$ and $D_{QPC}$ are (respectively) the source and drain of the QPC, and similarly, $S_{QD}$ and $D_{QD}$ are the source and drain of the quantum dot. The voltages associated with gates G1 and G2 can be varied to adjust the number $N$ of electrons on the dot one by one. On the left is a plot of the current through the dot $I_{dot}$, and the dc and differential conductances through the QPC (denoted by $G$ and $dG/dV_{G2}$) as the gate voltage $V_{G2}$ is varied. (Figure courtesy of K Ensslin.) Reprinted with permission from Schleser R, Ruh E, Ihn T, Ensslin K, Driscoll D C and Gossard A C 2004 *Appl. Phys. Lett.* **85** 2005. © 2004 American Institute of Physics.

must therefore be removed from the dot after transferring quantum information to the nuclear spin. In this case, the nuclear spin state may live as long as the nuclear spin dipole–dipole correlation time $\tau_{dd} \approx 10^{-4}$ s (in GaAs) or possibly longer if, for example, so-called WaHuHa NMR pulses are applied to suppress the dipole–dipole interaction [166].

## 4. Experimental achievements

In this section we present a selection of important experimental achievements leading towards the implementation of quantum information processing using electron spins in quantum dots.

### *4.1. Single and coupled quantum dots*

We first discuss different experimental approaches to construct semiconductor quantum dot structures that enable control over the spin degree of freedom on the level of a single electron. The precise control of the number of excess electrons in a quantum dot is a necessary prerequisite to achieve control over the spin states of interest. The addition of an electron from the surrounding material to a negatively charged dot requires the charging energy $\delta\epsilon_c$ to overcome the electrostatic energy of other electrons in the dot. The charging energy $\delta\epsilon_c$ depends on the number $N$ of charges confined in the dot. The regime (gate voltages) where the injection of additional electrons into the dot is blocked due to $\delta\epsilon_c$ is known as the Coulomb blockade regime (see figure 4). In recent years, a great deal of experimental effort has focused on the single-electron regime ($N = 1$) using different types of quantum dot structures. This regime provides experimental access to a spin 1/2 in the dot. There are several possibilities to produce quantum dot structures capable of confining single electrons. The list of ingenious quantum dot production techniques has grown enormously during the last years. Instead of presenting a complete list thereof, we rather focus on a few techniques that have paved the way for the first steps towards the implementation of quantum information processing using spin states.

As already mentioned in section 2.1, quantum dots can be created by electrical gating of a 2DEG via lithographically defined gate electrodes (see figures 1, 2, 5, and 6). Applying a negative voltage to the gates depletes the 2DEG underneath them, such that quantum dots are formed in the regions surrounded by the gates. Electrically gated dots are typically characterized by an electron level spacing $\delta\epsilon \approx 0.1 \ldots 2$ meV, a charging energy $\delta\epsilon_c \approx 1 \ldots 2$ meV, and a dot diameter $l \approx 10 \ldots 1000$ nm [169, 170]. Typical materials for such dots include GaAs, InSb, and Si. Control of the coupling of electrically gated GaAs quantum dots has been demonstrated and investigated in depth in transport experiments [170–172].

As an alternative to electrical gating, etching techniques [173] can also be applied to achieve lateral confinement in the plane of a 2DEG. For example, Tarucha *et al* [174] have produced gated vertical quantum dots by etching a pillar structure which contained a double-barrier heterostructure with an InGaAs quantum well as the 2DEG. Figures 7 and 12 show structures containing dots of this type.

Quantum dots also form 'naturally' at monolayer steps at the interface of, e.g., thin GaAs/AlGaAs quantum wells. Usually, molecular beam epitaxy (MBE) is used for the growth of such systems. If the MBE growth process is performed without interruption, such steps occur at random positions as natural fluctuations of the quantum well width. Quantum dots of this type possess excellent optical properties, including very sharp optical linewidths. This has allowed the coherent control of optically excited states in experiments [175, 176] and has recently culminated in the implementation of a CROT gate for qubits which are defined by the presence or absence of an exciton in the quantum dot [177].

Further, quantum dot structures can be grown by self-assembly, e.g., using the Stranski–Krastanov growth technique. In this technique, self-assembled dot islands form spontaneously during epitaxial growth due to a lattice

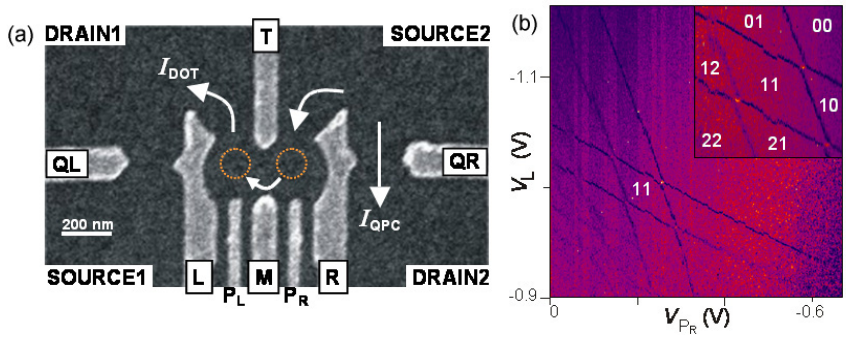


**Figure 5.** (a) Scanning electron micrograph of a gated double dot structure with two adjacent quantum point contacts (QPCs). The circles indicate the dot positions. When a bias voltage is applied between source 2 and drain 1, a current $I_{DOT}$ flows through the dots. Excess charges in the double dot modulate the current $I_{QPC}$ through one of the QPCs [168]. In this figure, the current $I_{QPC}$ flows from source 2 to drain 2 and enables charge readout via the right QPC. (b) Charge stability ('honeycomb') diagram of the double quantum dot. The labels $nm$ indicate the regions ('Coulomb diamonds') where $n$ ($m$) electrons are present in the left (right) dot. The colour scale indicates $\mathrm{d}I_{QPC}/\mathrm{d}V_L$, measured as a function of the bias voltages $V_L$ and $V_{P_R}$ applied to the gate L and the right plunger gate $P_R$, respectively. The inset shows a blow-up of the region around 11. (Figure courtesy of L P Kouwenhoven.) Reprinted with permission from Engel H-A, Kouwenhoven L P, Loss D and Marcus C M 2004 *Quantum Inf. Process.* **3** 115. © 2004 Springer-Verlag.

mismatch between the dot and the substrate material [178]. Typical sets of dot/substrate materials are InAs/GaAs, Ge/Si(100), GaN/AlN, InP/GaInP, and CdSe/ZnSe [179]. The electron level spacing of this type of dot is typically $\delta\epsilon \approx 30 \ldots 50$ meV with a charging energy $\delta\epsilon_c \approx 20$ meV, a diameter $l \approx 10 \ldots 50$ nm, and a height $d \approx 2 \ldots 10$ nm of the dot [180]. Small self-assembled dots typically have a pyramidal shape with four facets, whereas larger dots (containing, e.g., seven monolayers of InAs) form multi-faceted domes [179]. If pyramidal self-assembled dots are covered with a thin layer of the substrate material (called the capping layer), the capped dots take on an elliptical (or rarely, even a circular) shape. Additionally, these dots exert strain on the capping layer. If quantum dots are grown on the capping layer, they tend to grow on the strain field on top of the capped dots rather than at random positions. This enables the growth of vertically coupled quantum dots, where the thin capping layer acts as a barrier between the two dots (see figure 8(b)). A typical difficulty related to Stranski–Krastanov self-assembled dots is the intrinsic randomness of the growth process, as shown in figure 8(a). Yet, prepatterning of the substrate has been shown to be a way to achieve a well defined growth position of the first dot layer [181] (see figure 8(c)), paving the way to site-controlled arrays of single or coupled dots [182]. Cleaved-edge overgrowth is an alternative technique enabling atomically precise control of the growth site of single and coupled dots [183]. Colloidal chemistry is yet another promising approach to assemble quantum dots with well controlled size and shape [184]. Recently, colloidal CdSe dots have been coupled via molecular bridges [185]. The inter-dot coupling in these experiments mediated coherent spin transfer between the dots, which has subsequently been modelled theoretically [186].

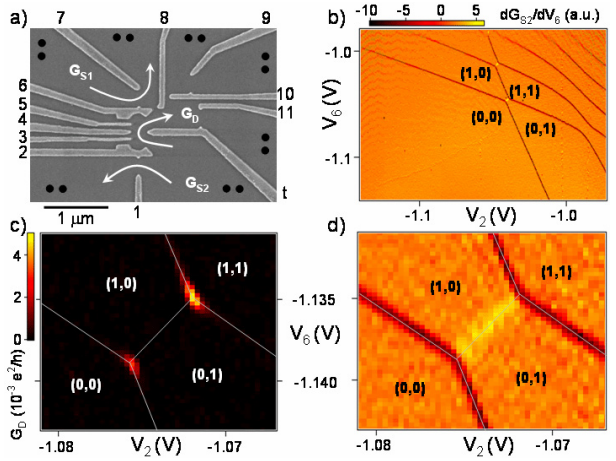


**Figure 6.** (a) SEM micrograph of an electrically gated double quantum dot structure with neighbouring QPC charge detectors [192]. The symbols • denote ohmic contacts. (b) Large-scale plot of the differential conductance $\mathrm{d}G_{S2}/\mathrm{d}V_6$ as a function of the voltages $V_2$ and $V_6$ applied to gates 2 and 6, respectively. The number of electrons is indicated by $(M, N)$, where $M(N)$ is the time-averaged number of electrons in the upper (lower) dot. In (c) and (d), $G_D$ and $\mathrm{d}G_{S2}/\mathrm{d}V_6$ are shown, respectively, as a function of $V_2$ and $V_6$ in the region close to the (1, 0) to (0, 1) transition. In (c) and (d), the gates have been slightly adjusted relative to (b) to allow simultaneous transport and sensing. In (b) and (d), identical colour scales are used. (Figure courtesy of C M Marcus.) Reprinted with permission from Petta J R, Johnson A C, Marcus C M, Hanson M P and Gossard A C 2004 *Phys. Rev. Lett.* **93** 186802. © 2004 by the American Physical Society.

### *4.2. Charge and spin control in quantum dots*

Precise control over the number of confined electrons has been demonstrated several years ago in InGaAs self-assembled dots [187], in gated vertical quantum dots [174], in quantum rings [188], and also in electrostatically defined single [189] and double [190–192] dots in GaAs. The single-electron states of quantum dots in the low-energy range have been shown to be in agreement with a shell model. Because the quantum dot confinement is much stronger along the growth direction than perpendicular to it (for dots defined in a 2DEG as well as for self-assembled dots), the dot potential is effectively two dimensional. The low-lying confined electron states can be well approximated by the states of a two-dimensional harmonic oscillator [174]. Thus, the single-particle ground state has

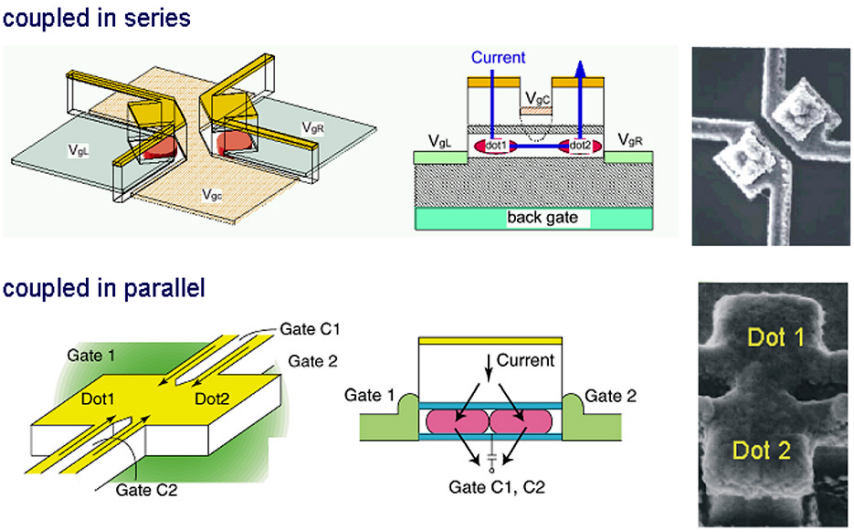


**Figure 7.** Different designs for etched structures of coupled quantum dots [240, 241]. The upper three figures show two quantum dots that can be probed by an electric current flowing through them in series, whereas the lower three pictures show two dots that are coupled in parallel for a transport experiment. The two rightmost figures are SEM micrographs. (Figure courtesy of W G van der Wiel.) Reprinted from Kodera T, van der Wiel W G, Ono K, Sasaki S, Fujisawa T and Tarucha S 2004 *Physica* E **22** 518; © 2004, with permission from Elsevier.

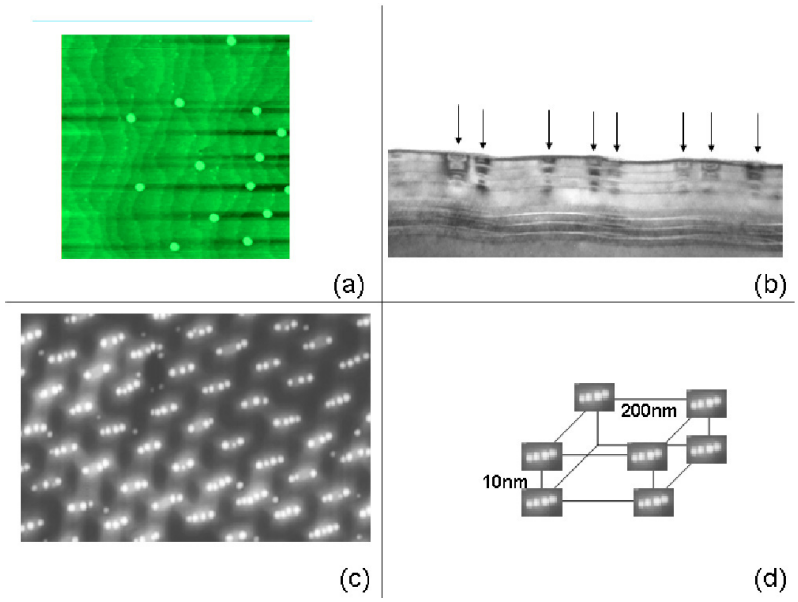


**Figure 8.** Self-assembled InAs quantum dot structures. (a) AFM picture of dots grown at random locations. (b) Transmission electron microscope (TEM) cross-section of vertically stacked dots (indicated by arrows), ordered along the growth axis. (c) AFM picture of laterally ordered dots. This image was generated after prepatterning of the substrate [181]. (d) Sketch of a three-dimensional lattice of dots that could be obtained by combining the growth methods of (b) and (c). (Figure courtesy of P M Petroff.)

s symmetry and the first excited shell has p symmetry. If an external magnetic field is applied perpendicular to the quantum dot plane, new harmonic oscillator states (Fock–Darwin states) are the exact eigenfunctions [193], with a frequency that increases with the magnetic field. Recently, Raymond *et al* [194] have observed the Fock–Darwin spectrum also for excitons (electron–hole pairs, rather than electrons alone) in quantum dots.

The degeneracy of the two spin states $|\uparrow\rangle$ and $|\downarrow\rangle$ is lifted in the presence of a magnetic field due to the Zeeman interaction. This makes the two states energetically distinguishable (see figure 9). The precise control of the occupation number of electrons in single and double quantum dots has enabled experiments on single spins in quantum dots, as we discuss in the following.

### *4.3. Spin relaxation*

Recently, expectations for the stability of spin qubits in quantum dots have grown considerably as progressively longer spin lifetimes have been reported. A series of works on electron spin relaxation in quantum dots started with Fujisawa *et al* [195] who reported a triplet-to-singlet relaxation time of $\tau_{S-T} = 200\ \mu s$ in vertical quantum dots. More recently, a lower bound on the singlet–triplet relaxation time has

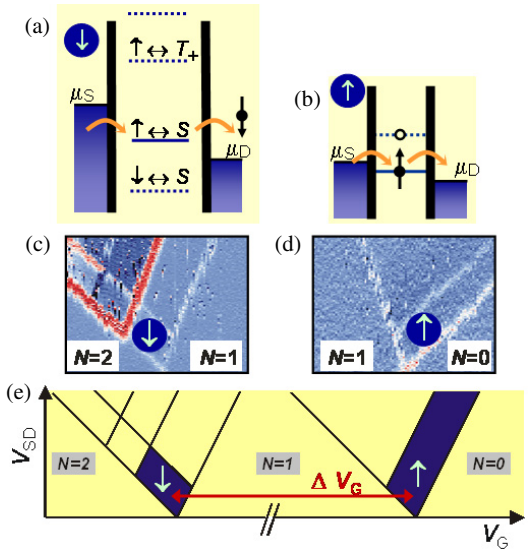


**Figure 9.** Quantum dot spin filter [198, 199] (see sections 4.3 and 4.5). A static magnetic field splits the spin states of the quantum dot due to the Zeeman interaction. For suitable gate voltages applied to the dot, the level configurations shown in (a) and (b) can be observed. In these cases, the transport through the dot is spin dependent for sequential tunnelling. (a) Only electrons in the state $|\downarrow\rangle$ are transported through the dot. They form an intermediate singlet state $|S\rangle$ with an excess electron (being in the excited Zeeman level) on the dot. Tunnelling of electrons with spin $|\uparrow\rangle$ through the dot is energetically not possible because there is no intermediate two-electron state available with an energy between the chemical potentials $\mu_S$ and $\mu_D$ of the source and the drain, respectively. (b) Only the spin ground state, $|\uparrow\rangle$, can pass through the (empty) dot. In (c) and (d), the measured differential conductance $dI/dV_{SD}$ is shown for cases (a) and (b), respectively, with tunnelling current $I$ and source–drain voltage $V_{SD}$. In (e), we show a scheme of the theoretically predicted $dI/dV_{SD}$ (which agrees well with (c) and (d)). (Figure courtesy of L P Kouwenhoven.) Reprinted with permission from Engel H-A, Kouwenhoven L P, Loss D and Marcus C M 2004 *Quantum Inf. Process.* **3** 115. © 2004 Springer-Verlag.

been measured in lateral dots, giving $\tau_{S-T} \geqslant 70\ \mu$s [196]. Very quickly thereafter, a substantially longer relaxation time ($\tau_{S-T} = (2.58 \pm 0.09)$ ms) was measured independently using a novel spin readout technique [197]. Several groups have since measured $T_1$ for *single* electron spins. For electrostatically defined GaAs dots, Hanson *et al* [198] have reported a lower bound $T_1 \gtrsim 50\ \mu$s at a magnetic field of $B = 7.5$ T which was subsequently topped by Elzerman *et al* [199], with $T_1 \approx (0.85 \pm 0.11)$ ms at $B = 8$ T. In these experiments, a two-level pulse technique for the quantum dot gate voltage has been applied to inject an electron into the dot and to extract it later. In a certain parameter range, the Zeeman splitting of the two spin states is sufficient that tunnelling into or out of the dot is not possible for one of the two spin states [200, 189, 195, 198] (see also figure 9). This enables spin detection via the detection of charge in the quantum dot, which has been realized through an adjacent quantum point contact (QPC) [168, 190, 198, 199] (in a set-up similar to that shown in figure 5(a) for a double quantum dot). In these experiments, the QPC has been tuned via a gate voltage to a conductance $G \approx e^2/h$, where the modulation of the current $I_{QPC}$ through the QPC has maximum sensitivity to changes in the electrostatic environment, including the number of charges in the quantum dot. Recently, Kroutvar *et al* [201] established a lower bound $T_1 \gtrsim 20$ ms at $T = 1$ K and $B = 4$ T for In(Ga)As self-assembled dots. In this experiment, an optical charge storage device has been excited with circularly polarized laser excitation. The larger level spacing of self-assembled dots (compared to gated GaAs dots) is responsible for the longer $T_1$-time seen in this experiment which is limited by spin–orbit coupling (see also section 3.3.1).

### *4.4. Spin decoherence*

The spin coherence of electrons localized at impurity centres has been investigated in depth for the last few decades in ensemble measurements. Many of these experiments have investigated the spin dephasing of electrons bound by the Coulomb interaction to a donor in silicon (for example, phosphorus, antimony, or arsenic). The wavefunction of such donor-bound electrons is quite similar to the wavefunction of electrons bound in a quantum dot. Several of these experiments have demonstrated rather long electron spin decoherence times, which is mainly due to the confinement of the electrons in all three spatial dimensions (leading to a $\delta$-peaked density of states). The electron nuclear double resonance (ENDOR) method has been applied to map out the wavefunction of the bound electron [202]. Hahn-echo measurements have shown that $T_2 \approx 10^{-4}$ s for donor electron spins in phosphorus-doped silicon (Si:P) [203]. Recent spin-echo measurements of isotopically purified $^{28}$Si:P have shown that $T_2 = 62$ ms [204]. This very long $T_2$-time is possible in such systems since $^{28}$Si has nuclear spin $I = 0$, drastically reducing the hyperfine interaction. In contrast, spin-echo measurements of electron spins bound to $^{29}$Si:P donors in isotopically purified $^{29}$Si have shown a much shorter envelope decay time (essentially $T_2$) on the order of $T_M \approx 10^{-5}$ s [205].

To our knowledge, there are only very few results published on measurements of the $T_2$ time of single electron spins in *quantum dots*. Still, optical experiments probing the decoherence time of *exciton* spins may provide a lower bound for the $T_2$-time of single electrons. Gupta *et al* [206] have measured a lower bound for the ensemble dephasing time of $T_2^* \approx 3$ ns for CdSe dots using femtosecond-resolved Faraday rotation. In this experiment, different decay timescales have been observed for the spin precession, showing a more complicated dynamics than expected. Recent $g$-factor calculations for electrons and holes in CdSe dots, based on time-dependent empirical tight-binding theory, addressed this issue [207]. A strongly anisotropic $g$-factor, with $g_x \approx g_y > g_z$ for all dot sizes (where $z$ denotes the $c$-axis of the wurtzite crystal), has been obtained for the electron. The range of $g$-factors (for the corresponding dot sizes) is in agreement with the experimentally [206] extracted pairs of $g$-factors, providing a first step in the understanding of the observed nontrivial dynamics of electron and hole spins in quantum dots. Measuring the Hanle effect in an ensemble of InAs self-assembled dots, Epstein *et al* [208] obtained $g_e T_2^* \approx 210$ ps at $T = 6$ K, where $g_e$ is the electron $g$-factor. In contrast to the single-spin decoherence time $T_2$, the ensemble dephasing time $T_2^*$ might be reduced from $T_2^* = T_2$ by dephasing among the spins of the measured ensemble. Further,

the electron–hole exchange interaction couples electron and hole spins in experiments that involve excitons. It can be assumed that this coupling further influenced the decay of the observed luminescence polarization. It might thus be possible that the coherence of single electron spins is larger than the values obtained from these experiments. In fact, recent Hanle measurements on individual quantum dots [161] have indicated an electron decoherence time $T_2 \approx 16$ ns. Yet, this result may have slightly exceeded the expected value $T_2 \approx \hbar\sqrt{N}/A$, discussed in section 3.3.2. The quantum dots in this experiment were defined by monolayer-high steps at the interfaces of a 3 nm thick GaAs/AlGaAs quantum well.

In section 5, we discuss further proposals to measure the $T_2$-time of a single electron spin in a quantum dot. Given the measured $T_1$ values in the millisecond range and measured $T_2$ times that are far smaller, it can be expected that nuclear spins are typically the dominant source of decoherence for electron spins in quantum dots.

### *4.5. Spin initialization*

To initialize the spin qubits, a strong polarization can be achieved by applying a strong magnetic field $B$, such that the Zeeman splitting is larger than the thermal energy, as already mentioned in section 2.1. Further, electrons with parallel spins can also be injected via spin-polarized currents. The injection of spins from ferromagnetic semiconductors into normal semiconductors has been reported with polarizations up to 90% [7, 8]. Initialization as well as detection of a single spin can also be achieved using a spin filter (see section 4.6) or by optical schemes (see section 4.9).

### *4.6. Single-spin detection*

A central question for the readout of a single spin is the reliability of the experimental result. We briefly address this issue here. Errors during the measurement process can be eliminated statistically by performing an experiment $n$ times identically. This procedure is called $n$-shot readout. There is a probability $p$ that the experimental readout procedure of a certain quantum mechanical state yields the correct result, and a probability $1 - p$ that it does not. In this way, one can define the probabilities $p_\uparrow$ and $p_\downarrow$ for the measurement successes of the states of a spin 1/2. Including the possibility of an error, the measurement of the state of a spin 1/2 is described by a measurement of the observables

$$A_\uparrow = p_\uparrow|\uparrow\rangle\langle\uparrow| + (1 - p_\downarrow)|\downarrow\rangle\langle\downarrow|, \tag{7}$$

$$A_\downarrow = p_\downarrow|\downarrow\rangle\langle\downarrow| + (1 - p_\uparrow)|\uparrow\rangle\langle\uparrow|, \tag{8}$$

where $A_\uparrow$ is the observable leading to the experimental result 'spin up', whereas $A_\downarrow$ leads to the result 'spin down'. To achieve a reliable measurement up to a significance level ('infidelity') $\alpha$, a statistical analysis of the readout process [209] yields the result that the number $n$ of required measurements has a lower bound

$$n > z_{1-\alpha}^2 \left(\frac{1}{\eta} - 1\right), \tag{9}$$

where $z_{1-\alpha}$ is the quantile (critical value) of the standard normal distribution function, $\Phi(z_{1-\alpha}) = 1 - \alpha = (1/2)[1 + \mathrm{erf}(z_{1-\alpha}/\sqrt{2})]$, and

$$\eta = \left(\sqrt{p_\uparrow p_\downarrow} - \sqrt{(1 - p_\uparrow)(1 - p_\downarrow)}\right)^2 \tag{10}$$

can be interpreted as a measurement efficiency with $\eta \in [0, 1]$. For example, if $p_\uparrow = 1 - p_\downarrow$, it is not possible to distinguish between the two spin states and $\eta = 0$. In contrast, for $p_\uparrow = p_\downarrow = 1$, the measurement is perfectly reliable and $\eta = 1$. The case $n = 1$ (which is realized, e.g., in the latter example) is called single-shot readout in the following. For a set of $k$ qubits, the probability for a reliable measurement is given by $1 - \beta = (1 - \alpha)^k$, where $\beta$ is the infidelity of the $k$-qubit readout. However, the number $n$ of required measurements only grows with $k$ according to $n \geqslant 2\,(1/\eta - 1)\log k/\beta$ [210]. The dependence of $n$ on $k$ is therefore weaker than what might be naively expected.

The magnetic moment of a single spin 1/2 is very small (on the order of $\mu_B = 9.2741 \times 10^{-24}$ J T$^{-1}$) and thus difficult to detect directly. Nevertheless, Rugar *et al* [81] have recently detected a single spin in silicon dioxide using MRFM, as already mentioned in section 2.7. MRFM enables the direct observation of an oscillating spin up to 100 nm below the surface with nanometre resolution. Still, the sensitivity is currently not yet sufficient to detect whether a spin is originally in the state $|\uparrow\rangle$ or in the state $|\downarrow\rangle$. Many other proposals to detect spin states are based on the transfer of information stored in the spin degree of freedom to an orbital degree of freedom ('spin-charge conversion') [9, 198–200, 211–214, 82, 215, 216]. Initialization and readout of spin states in quantum dots can be achieved, e.g., using a spin filter. This is a device that only transmits electrons with one particular spin polarization, while the opposite spin polarization is blocked. Recher *et al* [200] have proposed a spin-filter implementation consisting of a quantum dot in the Coulomb blockade regime, weakly coupled to two current leads. In a static magnetic field, the direction of the transmitted spin can be changed by tuning the gate voltage applied to the dot (see figures 9 and 10). Experimental demonstrations of a spin filter have been achieved by Folk *et al* [211], Potok *et al* [212], Hanson *et al* [198], and Elzerman *et al* [199]. The first two of these implementations have demonstrated the spin-filtering effect with a GaAs quantum dot in the open [211] and in the Coulomb-blockade regime [212] in a polarizer–analyser geometry (see also figure 10). In the polarizer–analyser geometry (see inset of figure 10), the spin-selective analyser was provided by a QPC with conductance tuned to less than $e^2/h$ [217]. A small perpendicular magnetic field $B_\perp$ coupled the polarizer (i.e., the quantum dot structure to the left) and the analyser (the QPC to the right) by transverse focusing. A transverse magnetic field $B_\parallel$ was applied, leading to a different Fermi wavelength of spin-up and spin-down electrons. By tuning the gate voltage of the dot, the transmission of one or the other spin was suppressed due to destructive interference of the coherent transport paths. With a constant current flowing between emitter (i.e., the dot) and collector (i.e., the QPC), peaks were observed in the voltage $V_c$ between collector and base whenever the distance between emitter and collector was an integer multiple of the cyclotron diameter of the transported

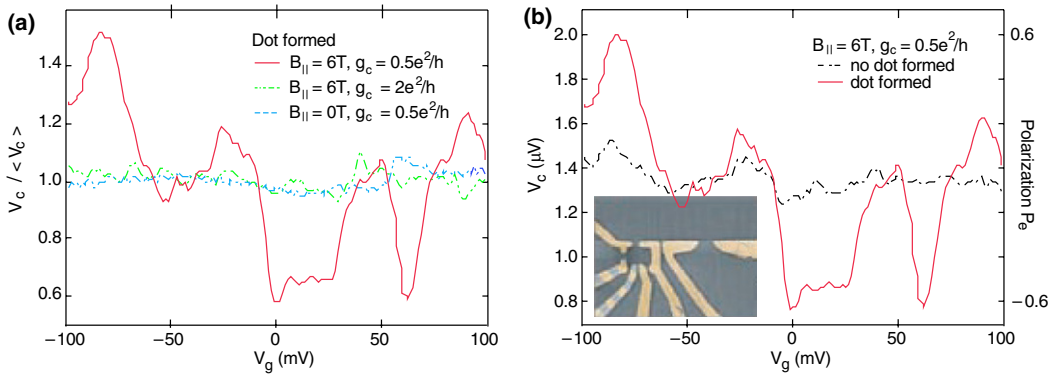


**Figure 10.** Experimental demonstration of a spin filter [211]. The inset shows a micrograph of the structure used, where the quantum dot on the left-hand side is the polarizer and the QPC on the right-hand side is the analyser. (a) and (b) show the focusing peak height as a function of the quantum dot gate voltage $V_g$. See section 4.6 for a description of the experiment. (a) Large fluctuations of the focusing peak height are measured at in-plane magnetic field $B_\parallel = 6$ T if the collector is spin selective (solid curve). These fluctuations are greatly reduced if the conductance of the QPC used as the collector is tuned out of the spin-selective regime [217] (dotted curve) or for zero in-plane magnetic field, $B_\parallel = 0$ (dashed curve). (b) The spin-filter effect is detectable at $B_\parallel = 6$ T with spin-selective collector when the emitter is a quantum dot (solid curve) and vanishes if the quantum dot is transformed into a QPC on the $2e^2/h$ plateau (dot–dashed curve). (Figure courtesy of C M Marcus.) Reprinted with permission from Engel H-A, Kouwenhoven L P, Loss D and Marcus C M 2004 *Quantum Inf. Process.* **3** 115. © 2004 Springer-Verlag.

electrons. In an in-plane magnetic field $B_\parallel$, the height of these peaks in $V_c$ (which are called 'focusing peaks') reflected the degree of spin polarization in the current if the QPC was in the spin-selective regime. The experiments by Hanson *et al* [198] and Elzerman *et al* [199] have already been described in section 4.3. Elzerman *et al* [199] demonstrated *single*-shot readout of a single electron spin in a quantum dot. A single-spin measurement of this type required a time ≈0.11 ms and the total fidelity of the spin readout was estimated to be 65%.

### *4.7. Optical interaction and optical readout of spins*

In this section, we first sketch some basics of optical transitions in quantum dots and then focus on the optical detection of spin states. The currently very active field of ultrafast laser technology suggests that single spin states can be optically detected and manipulated within very short times (picoseconds or even femtoseconds), several orders of magnitude faster than in schemes based on the transport of electric charge.

Via the absorption of a photon, an electron in a confined valence-band state can be excited to a confined conduction-band state. For such inter-band transitions, optical selection rules apply and establish conditions on the quantum numbers of the optically coupled states. Provided the spin–orbit interaction is nearly isotropic ($H_{so} \approx \lambda \mathbf{L}\cdot\mathbf{S}$, see also the discussion in section 3.3.1), then it is a good approximation that the total angular momentum squared, $\mathbf{J}^2 = (\mathbf{L}+\mathbf{S})^2$, provides a good quantum number in semiconductors. Photons with circular polarization $\sigma^\pm$ carry an angular momentum with projection $\pm 1$ (in units of $\hbar$) along their propagation direction. For optical interactions, the total angular momentum is conserved, linking the spin of electrons and the polarization of photons. For a two-dimensional quantum dot with circular confinement, the $z$-component $J_z$ of $\mathbf{J}$ is a good quantum number (in contrast, an anisotropic shape in the plane induces mixing of angular momentum eigenstates). When $J_z$ is a good quantum number in GaAs or InAs dots, the energetically lowest optical excitation at zero magnetic field typically includes two degenerate valence band states with total angular momentum projections $J_z = \pm 3/2$, which are also called heavy hole (hh) states. A circularly polarized photon that is irradiated along the quantization axis $z$ of $\mathbf{J}$ can excite one of the hh states to one of the conduction-band states with spin $+1/2$ or $-1/2$ [218]. For a given circular polarization, only one combination of these states satisfies the selection rules. This leads to a direct correspondence between the circular polarization of the photon and the spin of the optically excited electron. Taking advantage of this for the readout of spin states, light-emitting diodes ('spin LEDs') have been fabricated [7, 8], where the polarization of the emitted photons indicates the spin polarization of the electrons (or holes) injected into the spin LED. A further step in nanoscale photonic and electronic technology has been taken recently by the growth of semiconductor nanowire superlattices [219–221]. By modulating the reactants during catalytic growth of a nanowire, the nanowire finally consists of segments of different materials, e.g., Si and SiGe [219], InAs and InP [220], or GaAs and GaP [221]. By alternating the two different materials, a superlattice can be formed. The combination of n- and p-type semiconductors, e.g., n-Si and p-Si or n-InP and p-InP [221], enables the bottom-up assembly of nanoscale (spin) LEDs.

### *4.8. Negatively charged excitons in quantum dots*

Several methods have been developed to optically probe and manipulate states of *single* quantum dots [222, 223]. Optical schemes have further been proposed to achieve initialization of electron spins (see section 4.9), for the detection of the $T_2$-time of electron spins (see section 5.1), for single-qubit gates (see section 5.2), and for two-qubit gates (see section 5.3). In these schemes and also in many other schemes exploiting the spin states of an electron, a quantum dot initially contains a single excess electron. Optical excitation of such a state creates a negatively charged exciton (sometimes also called 'trion') in the dot, i.e., a compound of two conduction-band electrons and one valence-band hole (see figure 11). If the

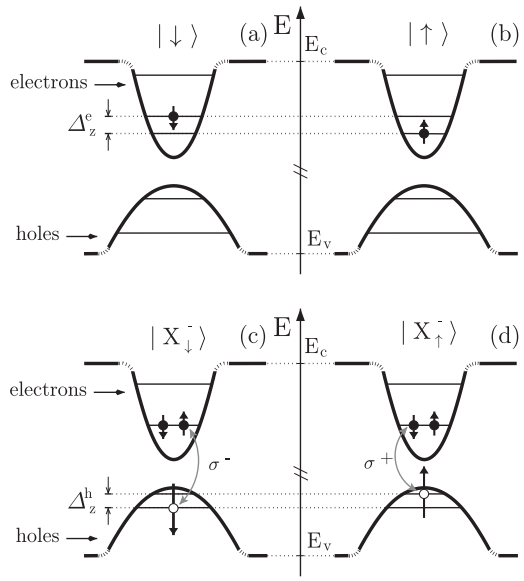


**Figure 11.** The two Zeeman states $|\downarrow\rangle$ and $|\uparrow\rangle$ of a single electron in the dot are shown in (a) and (b), whereas (c) and (d) show the two Zeeman states $|X^-_\uparrow\rangle$ and $|X^-_\downarrow\rangle$ of a negatively charged exciton in the orbital ground state [226, 229]. As discussed in the text, the two electrons in (c) and (d) form a spin singlet. The grey arrows indicate which electron–hole pair is coupled by a $\sigma^\pm$ circularly polarized transition. In the presence of a static magnetic field along the $z$ direction, the Zeeman splitting of the electron spin states is $\Delta^e_z$ and the Zeeman splitting of the charged exciton equals the hole Zeeman splitting $\Delta^h_z$. Here, we assume equal signs for the $g$-factors of electrons and holes.

quantum dot is in the so-called strong confinement regime, the (single-particle) confinement energies are much larger than the Coulomb interaction energies of the carriers in the dot. This criterion is typically satisfied for small self-assembled dots and colloidal dots. The two electrons then occupy the lowest single-particle level of the dot and form a spin singlet. Note that the excess electron initially occupies one of the available spin states. Due to the Pauli principle, the absorption of a circularly polarized photon (as described in section 4.7) is only possible if the corresponding electron spin state is not already occupied. Figure 11 shows that a $\sigma^-$-polarized photon can only be absorbed if the spin of the excess electron is in the state $|\downarrow\rangle$, whereas a $\sigma^+$-polarized photon can only be absorbed for $|\uparrow\rangle$. In the photoluminescence spectrum, the lines belonging to these two transitions coincide for zero magnetic field and split for non-zero magnetic fields. If a circularly polarized photon with an energy that matches the corresponding transition energy is absorbed, the initial spin state of the excess electron is identified. This experiment has recently been performed with a single InGaAs/GaAs dot by Högele *et al* [224] using high-resolution laser absorption spectroscopy. Equivalently, the photoluminescence (which is only emitted after a successful photon absorption) could be detected instead of the absorption. One can also apply an electric field to the dot such that an electron and a hole tunnel out of the dot after a photon has been absorbed. Instead of the photoluminescence, the resulting electric current (the so-called photocurrent) can then be detected [225]. For a discussion of the limits of such spin-dependent optical schemes due to the mixing of valence-band states, see section 4.9.

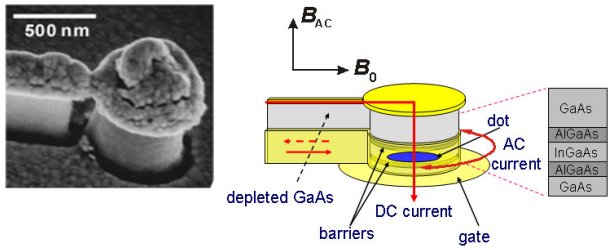


**Figure 12.** SEM picture and scheme of a structure to apply a local rf magnetic field to a quantum dot. Such a structure might be used as a prototype of a single qubit gate, or for the measurement of the electron spin decoherence time. The indicated AC current (in the horizontal direction) leads to an alternating magnetic field $B_{AC}$. In combination with a static magnetic field $B_0$, ESR can be induced with an electron located in the dot. From the modulation of the DC current (in the vertical direction) as a function of the frequency of the AC current, the electron spin decoherence time can be measured [215, 216]. (Figure courtesy of W G van der Wiel [242].)

### *4.9. Optical initialization of spin qubits*

The spin of an excess electron in a quantum dot can be polarized for initialization by using optical pumping methods [213, 214, 226]. As discussed in section 4.8, circularly polarized laser excitation can be used to optically address exclusively one of the two spin states $|\uparrow\rangle$ or $|\downarrow\rangle$. For initialization of a spin, the optical excitation can also be tuned to higher-lying continuum states [213]. Alternatively, applying circularly polarized optical $\pi$-pulses in the presence of a static (or pulsed) transverse magnetic field also increases the electron spin polarization [214]. In this scheme, the transverse magnetic field has a negligible effect on the charged exciton states because the in-plane $g$-factor of the hole is typically zero in first order (the response of the charged exciton to an external magnetic field is, in this case, determined by the hole spin since the two electrons form a singlet). A circularly polarized photon can now be absorbed for only, say, $|\downarrow\rangle$. After the absorption of a photon, the precession of the spin is locked until, after recombination, the initial spin state $|\downarrow\rangle$ is restored. The other electron spin state, $|\uparrow\rangle$, blocks the photon absorption and is therefore rotated by the transverse magnetic field without interruption. By choosing suitable pulse repetition rates and magnetic field strengths, the spin is polarized in the state $|\downarrow\rangle$. Yet another way to achieve electron spin polarization is to apply a magnetic field parallel to the laser beam and choose the circular polarization of the laser such that the hole contained in the charged exciton is in its excited Zeeman level, as shown in figure 11(c). Hole spin relaxation within the charged exciton (which occurs at elevated temperatures at even larger rates than those for optical recombination [227]) and subsequent recombination leads then to an increased polarization of the electron spin in the state $|\uparrow\rangle$ that does not allow photon absorption [226] (in contrast to the scheme mentioned above). To benefit from Pauli blocking of the absorption in these schemes, the bandwidth of the laser must be smaller than the splitting of hh and, typically, light hole (lh) states (which have angular momentum $J_z = \pm 1/2$) and also the energy difference to the state with one electron in the first excited level, forming a triplet state with the electron in the orbital ground state. For self-assembled dots, this hh–lh splitting is on the order of 10 meV, and the energy

difference from the mentioned state with an electron triplet is approximately 40 meV [213].

In the context of optical transitions including hh and lh states it has turned out that the geometry of the quantum dot can also impose a limitation on the efficiency of spin-dependent optical processes. As already mentioned in section 4.1, capped self-assembled dots are elliptical, rather than circular in shape. This anisotropy leads to a mixing especially of the valence band states (since they are close in energy to each other). If the bandwidth of the circularly polarized laser is larger than the Zeeman splitting of the electron states, the admixture of, e.g., lh states with the hh states (as in bulk semiconductors) increases the probability that a photon is absorbed even though the spin is in the state where Pauli blocking should be effective [218]. However, if a circularly polarized laser with a bandwidth smaller than the electron Zeeman splitting is applied in resonant optical experiments [224], the mixing of the hole states has no effect on the absorption properties of the quantum dot because then, again, only one of the electron spin states allows for photon absorption.

## 5. Future goals

In this section we discuss recent theoretical proposals to measure the $T_2$ time of single electron spins in quantum dots and also proposals for single-qubit rotations.

### *5.1. Detection of single-electron spin decoherence*

After the recent successful measurements of the $T_1$-lifetime (and lower bounds for it) of single electron spins in quantum dots (see section 4.3), measurements of the decoherence time $T_2$ are due. To achieve such an experiment, an initial coherent evolution of the electron spin must be produced. This can be done, e.g., with electron spin resonance (ESR) or by inducing spin precession in a transverse magnetic field. The decay of the spin coherence can then be measured [161]. Several proposals of this type have been made. Engel and Loss [215, 216] have proposed a measurement of the sequential tunnelling current through a dot containing a single electron spin in the presence of ESR excitation. Sequential tunnelling, in general, describes a regime where charge transport only occurs via a sequence of first-order tunnelling processes. In the regime when sequential tunnelling is only possible via an intermediate singlet state on the dot [215, 216], the stationary current $I$ is a Lorentzian as a function of the ESR detuning $\delta_{\mathrm{ESR}} = \omega_{\mathrm{ESR}} - g_{\mathrm{e}}\mu_{\mathrm{B}}B$, where $\omega_{\mathrm{ESR}}$ is the ESR frequency. The inverse of the linewidth of $I(\delta_{\mathrm{ESR}})$ provides a lower bound for the intrinsic $T_2$ time of a single electron spin. Further, the coherent Rabi oscillations due to ESR pulses can be observed in the time-averaged current $\bar{I}(t_{\mathrm{p}})$ as a function of the ESR pulse length $t_{\mathrm{p}}$. Subsequently, Martin *et al* [228] have proposed the electrical detection of single-electron spin resonance via a nearby field-effect transistor conduction channel. In contrast to a transport measurement, Gywat *et al* [226, 229] have theoretically studied the optical detection of magnetic resonance (ODMR) to measure the $T_2$-time of a single electron spin in a quantum dot. In this approach, the dot initially contains a single excess electron that is subject to ESR excitation. Unlike a tunnelling experiment [215, 216, 228], optical transitions are subject to selection rules and are not restricted to the Coulomb blockade regime, e.g., if the excess electron is present due to n doping and is not electrically injected. Further, an ODMR experiment can be performed without connecting the dot to current leads, which reduces decoherence. One can additionally benefit from the high sensitivity of photodetectors. For a $\sigma^-$-polarized laser with a sufficiently low bandwidth the absorption of a photon is Pauli blocked if the spin is in the state $|\uparrow\rangle$, as discussed in section 4.8 (see also figure 11). The laser frequency and polarization ($\sigma^-$) in the considered ODMR scheme are adjusted such that in the case of successful photon absorption a negatively charged exciton, as shown in figure 11(c), is created, where the two electrons form a singlet and the hole is in the excited Zeeman level of the orbital ground state. From here, there are two possible relaxation paths, either the direct optical recombination, or a hole spin flip and an optical transition with opposite circular polarization. This second relaxation channel is responsible for an accumulation of population in the spin ground state (exactly as discussed in section 4.9 for spin initialization) since the optical recombination rate is usually much faster than the ESR Rabi frequency. For cw ESR and cw laser excitations, the stationary photoluminescence [226] or, alternatively, the stationary photocurrent [229] has been found to be a Lorentzian as a function of the ESR detuning $\delta_{\mathrm{ESR}}$. As in the detection of the ESR linewidth using sequential tunnelling, the inverse linewidth of the photoluminescence or the photocurrent provides a lower bound for $T_2$. Additional broadening due to the optical transitions is greatly reduced for a hole spin-flip rate that is comparable to or larger than the optical recombination rate, as well as for an optical Rabi frequency on the order of $1/T_2$ or smaller. Alternatively, pulsed laser excitation can be applied in addition to an ESR excitation. This enables the detection of spin Rabi oscillations as a function of the laser pulse repetition time $\tau_{\mathrm{rep}}$. Because of hole spin flips, the electron spin at the end of a laser pulse is polarized as mentioned above. During the 'off'-time of the laser, the spin is performing Rabi oscillations. When the subsequent laser pulse arrives, the spin state $|\downarrow\rangle$ is read out. The time-averaged number of photons that are emitted per laser repetition period then directly displays the electron spin Rabi oscillations as a function of $\tau_{\mathrm{rep}}$. Increasing the length of the laser pulses to values longer than the exciton lifetime iterates the optical pumping scheme and therefore enhances its efficiency. This results in an improved visibility of the oscillations in the photoluminescence or in the photocurrent. Using the same optical excitation set-up, electron spin precession can also be observed in the presence of a transverse magnetic field [229].

### *5.2. Single-qubit rotations*

A further important step towards the goal of quantum computation is the implementation of a single-qubit gate. To achieve this for the Loss–DiVincenzo proposal, several possible strategies have been developed [9, 88, 1]. The simplest way to rotate a spin is by applying a pulsed magnetic field. In an array of quantum dots, such fields could be applied to single spins, e.g., by scanning-probe tips [9]. Further, in the presence of an rf magnetic field applied to an ensemble of electron spins, the tunability and precise control of the

individual Zeeman splittings is sufficient to produce single spin rotations, as already mentioned in section 2.1. When the ESR resonance condition is matched, the spin rotates with maximum amplitude, according to the well known Rabi formula. Detuning of the Zeeman splitting of an individual spin from the ESR resonance slows its precession frequency and the spin stops rotating entirely when the detuning is larger than the ESR linewidth. Control of the Zeeman splitting at the single-spin level is therefore another way to perform single-spin rotations. This can be achieved in principle by controlling local magnetic fields or local Overhauser fields. For a structure designed to apply ESR excitation to a single quantum dot, see figure 12. Another approach is the individual control of the electron $g$-factor instead of the local magnetic field. In quantum wells, there has been recent pioneering work in this direction [230–232]. Salis *et al* [230] have demonstrated electrically controlled modulation of the $g$-factor in an AlGaAs quantum well containing a gradient in the Al concentration. Here, the electron wavefunction was shifted between regions with different Al concentration via applied gate voltages, which resulted in the observation of a different electron $g$-factor. Kato *et al* [231] have even demonstrated voltage-controlled modulation of the $g$-tensor. This allows the induction of ESR without time-dependent magnetic fields. Further experiments by Kato *et al* [232] exploited the spin–orbit interaction to achieve coherent spin manipulation in strained semiconductor films without the application of magnetic fields.

Alternative proposals to produce single-spin rotations are related to all-optical Raman transitions [25] and stimulated Raman adiabatic passage (STIRAP) [25, 92, 233, 234], a method based on two-photon Raman transitions which has already been applied to atoms and molecules to transfer a precisely controlled population between two quantum states [235]. While Troiani *et al* [92] have also considered the realization of conditional and unconditional quantum gates using an additional adjacent quantum dot, Chen *et al* [233] have proposed a STIRAP process with no auxiliary state, but in the presence of a transverse magnetic field. In this set-up, control of the relative phase and the relative intensity of two applied laser pulses enables an arbitrary spin rotation for a given polarization of the light and direction of the transverse magnetic field [233]. As an alternative method of performing a spin rotation on an excess electron confined to a quantum dot, Calarco *et al* [234] have proposed to excite lh states via a sequence of a linearly and then a circularly polarized laser $\pi$-pulse. Given this abundance of proposals for single-qubit gates, there is great hope for working experimental realizations in the near future.

### *5.3. Two-qubit gates*

Swapping of the spin states of two electrons located in closely spaced quantum dots seems by now to be a realistic first experimental step towards a two-qubit gate for spins. As explained in section 2.1, this can be achieved by controlling the overlap of the two wavefunctions of the electrons and thus the singlet–triplet splitting $J$. The interdot tunnel splitting and $J$ can be determined from a transport experiment in the sequential tunnelling regime [236–238]. Recently, $J$ has been measured for two electrons in a single gated quantum dot by detecting inelastic cotunnelling above and below a magnetic-field-driven singlet–triplet transition [116]. In the cotunnelling regime, only second-order tunnelling processes contribute to charge transport. Because the dot was elliptical, a two-electron wavefunction similar to that in a double dot was expected. Two different samples yielded $J \approx 0.2$ meV and $J \approx 0.57$ meV at $B = 0$. The critical magnetic field for the singlet–triplet transition (where $J = 0$) has been measured to be $B^* \approx 1.3$ T. For the interaction parameter [238], $\phi \approx 0.5 \pm 0.1$ has been obtained, indicating that the ground state given by $|{+}\uparrow, {+}\downarrow\rangle - \phi|{-}\uparrow, {-}\downarrow\rangle/\sqrt{1+\phi^2}$ (where $\pm$ stands for the symmetric/antisymmetric orbital wavefunction) consists of a singlet with a significant admixture of single-electron orbitals due to the electron–electron interaction. The entanglement of the two electron spins in the state above can be quantified by the concurrence $C = 2\phi/(1+\phi^2)$ [238, 40]. The experimental result $C \approx 0.8$ shows that electron–electron interaction reduces the degree of spin entanglement from its maximum ($C = 1$), which is obtained for a singlet (having $\phi = 1$). This demonstration strongly encourages the view that similar results might be soon obtained in double dots (which are needed for spatially separating the two qubits).

In addition to the two-qubit gate that is controlled via the tunnel coupling of the two dots (see section 2.1), there is also a proposal for an optical two-qubit phase gate [234]. In this proposal, a two-qubit phase gate is established by applying an adiabatically chirped laser pulse (this is a pulse with a time-dependent frequency) to two neighbouring quantum dots, each with one excess electron. The desirable phase of the two-qubit gate is accumulated during the (electrostatic) interaction time of the two charged excitons that are excited in the two dots. The adiabatic change of the laser detuning protects the system from interaction with phonons, even in the presence of hole-state mixing. The combination of such a two-qubit gate with an optical single-qubit gate (as outlined in section 5.2) would finally enable all-optical quantum computation using spins in quantum dots.

## 6. Conclusions

In this tutorial we have discussed theoretical concepts and the present status of experimental achievements towards the implementation of quantum information processing using electron spins in quantum dots. The demonstration of working single- and two-qubit gates and finally the production of quantum dot arrays that enable the application of an entire quantum algorithm including error correction are the major problems to tackle towards the goal of a solid-state implementation of quantum information processing using electron spins in quantum dots.

## Acknowledgments

We thank D N Bulaev, H A Engel, K Ensslin, S I Erlingsson, V N Golovach, A Högele, L P Kouwenhoven, J Lehmann, C M Marcus, P M Petroff and W G van der Wiel for useful discussions and for supplying valuable material to this work. We acknowledge support from the NCCR Nanoscience, the Swiss NSF, NSERC of Canada, EU RTN Spintronics, EU RTN QUEMOLNA, DARPA, ARO, and ONR.

## References


[1] Awschalom D D, Loss D and Samarth N 2002 *Semiconductor Spintronics and Quantum Computation* (Berlin: Springer)
[2] Žutić I, Fabian J and Das Sarma S 2004 *Rev. Mod. Phys.* **76** 323
[3] Baibich M N, Broto J M, Fert A, Nguyen Van Dau F, Petroff F, Etienne P, Creuzet G, Friederich A and Chazeles J 1998 *Phys. Rev. Lett.* **61** 2472
[4] Datta S and Das B 1990 *Appl. Phys. Lett.* **56** 665
[5] Kikkawa J M, Smorchkova I P, Samarth N and Awschalom D D 1997 *Science* **277** 1284
[6] Kikkawa J M and Awschalom D D 1998 *Phys. Rev. Lett.* **80** 4313
[7] Fiederling R, Keim M, Reuscher G, Ossau W, Schmidt G, Waag A and Molenkamp L W 1999 *Nature* **402** 787
[8] Ohno Y, Young D K, Beschoten B, Matsukura F, Ohno H and Awschalom D D 1999 *Nature* **402** 790
[9] Loss D and DiVincenzo D P 1998 *Phys. Rev.* A **57** 120 (*Preprint* cond-mat/9701055)
[10] Feynman R 1985 *Quantum Mechanical Computers Opt. News* (Feb.) 11
[11] Deutsch D 1985 *Proc. R. Soc.* A **400** 97
[12] Deutsch D and Jozsa R 1992 *Proc. R. Soc.* A **439** 553
[13] Shor P W 1994 *Proc. 35th Symp. on the Foundations of Computer Science* (Los Alamitos, CA: IEEE Computer Society Press) p 124
[14] Shor P W 1997 *SIAM J. Sci. Stat. Comput.* **26** 1484 (*Preprint* quant-ph/9508027)
[15] Grover L K 1997 *Phys. Rev. Lett.* **79** 325
[16] Gershenfeld N A and Chuang I L 1997 *Science* **275** 350
[17] Kane B E 1998 *Nature* **393** 133
[18] Cirac J I and Zoller P 1995 *Phys. Rev. Lett.* **74** 4091
[19] Shnirman A, Schön G and Hermon Z 1997 *Phys. Rev. Lett.* **79** 2371
[20] Preskill J http://www.theory.caltech.edu/people/preskill/ph229/
[21] Barenco A, Bennett C H, Cleve R, DiVincenzo D P, Margolus N, Shor P, Sleator T, Smolin J A and Weinfurter H 1995 *Phys. Rev.* A **52** 3457
[22] DiVincenzo D P 2000 *Fortschr. Phys.* **48** 771
[23] Averin D V 1998 *Solid State Commun.* **105** 659
[24] Privman V, Vagner I D and Kventsel G 1998 *Phys. Lett.* A **239** 141
[25] Imamoğlu A, Awschalom D D, Burkard G, DiVincenzo D P, Loss D, Sherwin M and Small A 1999 *Phys. Rev. Lett.* **83** 4204
[26] Meier F, Levy J and Loss D 2003 *Phys. Rev. Lett.* **90** 047901
[27] Levy J 2001 *Phys. Rev.* A **64** 052306
[28] Ladd T D, Goldman J R, Yamaguchi F, Yamamoto Y, Abe E and Itoh K M 2002 *Phys. Rev. Lett.* **89** 017901
[29] Friesen M, Rugheimer P, Savage D E, Lagally M G, van der Weide D W, Joynt R and Eriksson M A 2003 *Phys. Rev.* B **67** 121301(R)
[30] Stoneham A M, Fisher A J and Greenland P T 2003 *J. Phys.: Condens. Matter* **15** L447
[31] Domokos P, Raimond J M, Brune M and Haroche S 1995 *Phys. Rev.* A **52** 3554
[32] Turchette Q A, Hood C J, Lange W, Mabuchi H and Kimble H J 1995 *Phys. Rev. Lett.* **75** 4710
[33] Monroe C, Meekhof D M, King B E, Itano W M and Wineland D J 1995 *Phys. Rev. Lett.* **75** 4714
[34] Schmidt-Kaler F, Häffner H, Riebe M, Gulde S, Lancaster G P T, Deuschle T, Becher C, Roos C F, Eschner J and Blatt R 2003 *Nature* **422** 408
[35] Vandersypen L M K, Steffen M, Breyta G, Yannoni C S, Sherwood M H and Chuang I L 2001 *Nature* **414** 883
[36] Brennen G K, Caves C M, Jessen P S and Deutsch I H 1999 *Phys. Rev. Lett.* **82** 1060
[37] Duan L-M, Demler E and Lukin M D 2003 *Phys. Rev. Lett.* **91** 090402
[38] Wu L-A, Lidar D A and Friesen M 2004 *Phys. Rev. Lett.* **93** 030501
[39] Medeiros-Ribeiro E, Ribeiro E and Westfahl H 2003 *Appl. Phys.* A **77** 725
[40] Schliemann J, Loss D and MacDonald A H 2001 *Phys. Rev.* B **63** 085311
[41] Schliemann J and Loss D 2003 *Proc. Int. School of Physics 'E. Fermi': Quantum Phenomena in Mesoscopic Systems* (Amsterdam: IOS Press) p 135 (*Preprint* cond-mat/0212141)
[42] Requist R, Schliemann J, Abanov A G and Loss D 2004 *Preprint* cond-mat/0409096
[43] Mooij J E, Orlando T P, Levitov L, Tian L, van der Wal C H and Lloyd S 1999 *Science* **285** 1036
[44] Orlando T P, Mooij J E, Tian L, van der Wal C H, Levitov L S, Lloyd S and Mazo J J 1999 *Phys. Rev.* B **60** 15398
[45] Makhlin Y, Schön G and Shnirman A 1999 *Nature* **398** 305
[46] Schön G and Zaikin A D 1990 *Phys. Rep.* **198** 237
[47] Ioffe L B, Geshkenbein V B, Feigel'man M V, Fauchère A L and Blatter G 1999 *Nature* **398** 679
[48] Zagoskin A M 2002 *Physica* C **368** 305
[49] Chtchelkatchev N M and Nazarov Yu V 2003 *Phys. Rev. Lett.* **90** 226806
[50] Vion D, Aassime A, Cottet A, Joyez P, Pothier H, Urbina C, Esteve D and Devoret M H 2002 *Science* **296** 886
[51] Yang Y, Han S, Chu X, Chu S and Wang Z 2002 *Science* **296** 889
[52] Yamamoto T, Pashkin Yu A, Astafiev O, Nakamura Y and Tsai J S 2003 *Nature* **425** 941
[53] Wallraff A, Schuster D I, Blais A, Frunzio L, Huang R-S, Majer J, Kumar S, Girvin S M and Schoelkopf R J 2004 *Nature* **431** 162
[54] Burkard G, Koch R H and DiVincenzo D P 2004 *Phys. Rev.* B **69** 064503
[55] Tian L, Lloyd S and Orlando T P 2002 *Phys. Rev.* B **65** 144516
[56] Meier F and Loss D 2004 *Preprint* cond-mat/0408594
[57] Makhlin Y, Schön G and Shnirman A 2001 *Rev. Mod. Phys.* **73** 357
[58] Burkard G 2004 *Preprint* cond-mat/0409626
[59] Vagner I D and Maniv T 1995 *Physica* B **204** 141
[60] Mozyrsky D, Privman V and Glasser M L 2001 *Phys. Rev. Lett.* **86** 5112
[61] Mozyrsky D, Privman V and Vagner I D 2001 *Phys. Rev.* B **63** 085313
[62] de Sousa R, Delgado J D and Das Sarma S 2004 *Phys. Rev.* A **70** 052304
[63] Koiller B, Hu X and Das Sarma S 2002 *Phys. Rev. Lett.* **88** 027903
[64] DiVincenzo D P, Bacon D, Kempe J, Burkard G and Whaley K B 2000 *Nature* **408** 339
[65] Friedman J R, Sarachik M P, Tejada J and Ziolo R 1996 *Phys. Rev. Lett.* **76** 3830
[66] Wernsdorfer W and Sessoli R 1999 *Science* **284** 133
[67] del Barco E, Kent A D, Yang E C and Hendrickson D N 2004 *Phys. Rev. Lett.* **93** 157202
[68] Leuenberger M N, Meier F and Loss D 2003 *Monats. Chem.* **134** 217
[69] Hill S, Edwards R S, Aliaga-Alcalde N and Christou G 2003 *Science* **302** 1015
[70] Troiani F, Ghirri A, Affronte M, Caretta S, Santini P, Amoretti G, Piligkos S, Timco G and Winpenny R E P 2004 *Preprint* cond-mat/0405507
[71] Leuenberger M N and Loss D 2001 *Nature* **410** 789
[72] Leuenberger M N, Loss D, Poggio M and Awschalom D D 2002 *Phys. Rev. Lett.* **89** 207601
[73] Leuenberger M N and Loss D 2003 *Phys. Rev.* B **68** 165317
[74] Claudon J, Balestro F, Hekking F W J and Buisson O 2004 *Phys. Rev. Lett.* **93** 187003
[75] Ahn J, Weinacht T C and Bucksbaum P H 2000 *Science* **287** 463

[76] Troiani F, Affronte M, Caretta S, Santini P and Amoretti G 2004 *Preprint* cond-mat/0411113
[77] Recher P, Loss D and Levy J 2000 *Proc. Macroscopic Quantum Coherence and Computing* ed D Averin and P Silvestrini (New York: Plenum) (*Preprint* cond-mat/0009270)
[78] Abe E, Itoh K M, Ladd T D, Goldman J R, Yamaguchi F and Yamamoto Y 2003 *J. Supercond.* **16** 175
[79] Rugar D, Yannoui C S and Sidles J A 1992 *Nature* **360** 563
[80] Berman G P, Doolen G D, Hammel P C and Tsifrinovich V I 2000 *Phys. Rev.* B **61** 14694
[81] Rugar D, Budakian R, Mamin H J and Chui B W 2004 *Nature* **430** 329
[82] Friesen M, Tahan C, Joynt R and Eriksson M A 2004 *Phys. Rev. Lett.* **92** 037901
[83] Stoneham A M 2003 *Physica* B **340** 48
[84] Rodriquez R, Fisher A J, Greenland P T and Stoneham A M 2004 *J. Phys.: Condens. Matter* **16** 2757
[85] DeMarco B *et al* 2002 *Phys. Rev. Lett.* **89** 267901
[86] Tian L, Rabl P, Blatt R and Zoller P 2004 *Phys. Rev. Lett.* **92** 247902
[87] DiVincenzo D P and Loss D 1999 *J. Magn. Magn. Mater.* **200** 202
[88] Burkard G, Loss D and DiVincenzo D P 1999 *Phys. Rev.* B **59** 2070
[89] Gywat O, Burkard G and Loss D 2002 *Phys. Rev.* B **65** 205329
[90] Leuenberger M N, Flatté M E and Awschalom D D 2003 *Preprint* cond-mat/0307657
[91] Leuenberger M N, Flatté M E and Awschalom D D 2004 *Preprint* cond-mat/0407499
[92] Troiani F, Molinari E and Hohenester U 2003 *Phys. Rev. Lett.* **90** 206802
[93] Cerletti V, Gywat O and Loss D 2004 *Preprint* cond-mat/0411235
[94] Beenakker C W J, DiVincenzo D P, Emary C and Kindermann M 2004 *Phys. Rev. Lett.* **93** 020501
[95] Stace T M, Barnes C H W and Milburn G J 2004 *Phys. Rev. Lett.* **93** 126804
[96] Burkard G, Loss D and Sukhorukov E V 2000 *Phys. Rev.* B **61** R16303
[97] Loss D and Sukhorukov E V 2000 *Phys. Rev. Lett.* **84** 1035
[98] Egues J C, Burkard G and Loss D 2002 *Phys. Rev. Lett.* **89** 176401
[99] Burkard G and Loss D 2003 *Phys. Rev. Lett.* **91** 087903
[100] Samuelsson P, Sukhorukov E V and Büttiker M 2004 *Phys. Rev.* B **70** 115330
[101] Recher P, Sukhorukov E V and Loss D 2001 *Phys. Rev.* B **63** 165314
[102] Lesovik G B, Martin T and Blatter G 2001 *Eur. Phys. J.* B **24** 287
[103] Mélin R 2001 *Preprint* cond-mat/0105073
[104] Costa A T Jr and Bose S 2001 *Phys. Rev. Lett.* **87** 277901
[105] Oliver W D, Yamaguchi F and Yamamoto Y 2002 *Phys. Rev. Lett.* **88** 037901
[106] Bose S and Home D 2002 *Phys. Rev. Lett.* **88** 050401
[107] Recher P and Loss D 2002 *Phys. Rev.* B **65** 165327
[108] Bena C, Vishveshwara S, Balents L and Fisher M P A 2002 *Phys. Rev. Lett.* **89** 037901
[109] Saraga D S and Loss D 2003 *Phys. Rev. Lett.* **90** 166803
[110] Bouchiat V, Chtchelkatchev N, Feinberg D, Lesovik G B, Martin T and Torrès J 2003 *Nanotechnology* **14** 77
[111] Recher P and Loss D 2003 *Phys. Rev. Lett.* **91** 267003
[112] Saraga D S, Altshuler B L, Loss D and Westervelt R M 2004 *Phys. Rev. Lett.* **92** 246803
[113] Samuelsson P, Sukhorukov E V and Büttiker M 2003 *Phys. Rev. Lett.* **91** 157002
[114] Beenakker C W J, Emary C, Kindermann M and van Velsen J L 2003 *Phys. Rev. Lett.* **91** 147901
[115] Samuelsson P, Sukhorukov E V and Büttiker M 2004 *Phys. Rev. Lett.* **92** 026805
[116] Zumbühl D M, Marcus C M, Hanson M P and Gossard A C 2004 *Phys. Rev. Lett.* **93** 256801
[117] Egues J C, Recher P, Saraga D S, Golovach V N, Burkard G, Sukhorukov E V and Loss D 2003 *Quantum Noise in Mesoscopic Physics* vol 97, ed Yu V Nazarov (Dordrecht: Kluwer) p 241 (*Preprint* cond-mat/0210498)
[118] Recher P, Saraga D S and Loss D 2004 *Fundamental Problems of Mesoscopic Physics: Interaction and Decoherence* (*NATO Science Ser. II vol 154,* ) ed I V Lerner *et al* (Dordrecht: Kluwer) p 179 (*Preprint* cond-mat/0408526)
[119] Hu X and Das Sarma S 2000 *Phys. Rev.* A **61** 062301
[120] Barrett S D and Barnes C H W 2002 *Phys. Rev.* B **66** 125318
[121] Steane A M 2003 *Phys. Rev.* A **68** 042322
[122] Mizel A and Lidar D A 2004 *Phys. Rev. Lett.* **92** 077903
[123] Loss D and DiVincenzo D P 2003 *Preprint* cond-mat/0304118
[124] DiVincenzo D P and Loss D 2005 *Phys. Rev.* B **71** 035318
[125] Miller J B, Zumbühl D M, Marcus C M, Lyanda-Geller Y B, Goldhaber-Gordon D, Campman K and Gossard A C 2003 *Phys. Rev. Lett.* **90** 076807
[126] Paget D, Lampel G, Sapoval B and Safarov V I 1977 *Phys. Rev.* B **15** 5780
[127] DiVincenzo D P and Loss D 1998 *Superlattices Microstruct.* **23** 419
[128] Khaetskii A V and Nazarov Yu V 2000 *Phys. Rev.* B **61** 12639
[129] Khaetskii A V and Nazarov Yu V 2001 *Phys. Rev.* B **64** 125316
[130] Levitov L S and Rashba E I 2003 *Phys. Rev.* B **67** 115324
[131] Glavin B A and Kim K W 2003 *Phys. Rev.* B **68** 045308
[132] Cheng J L, Wu M W and Lü C 2004 *Phys. Rev.* B **69** 115318
[133] Golovach V N, Khaetskii A and Loss D 2004 *Phys. Rev. Lett.* **93** 016601
[134] Erlingsson S I, Nazarov Yu V and Fal'ko V I 2001 *Phys. Rev.* B **64** 195306
[135] Erlingsson S I and Nazarov Yu V 2002 *Phys. Rev.* B **66** 155327
[136] Khaetskii A V, Loss D and Glazman L 2002 *Phys. Rev. Lett.* **88** 186802
[137] Khaetskii A V, Loss D and Glazman L 2003 *Phys. Rev.* B **67** 195329
[138] Schliemann J, Khaetskii A V and Loss D 2002 *Phys. Rev.* B **66** 245303
[139] Merkulov I A, Efros Al L and Rosen M 2002 *Phys. Rev.* B **65** 205309
[140] de Sousa R and Das Sarma S 2003 *Phys. Rev.* B **67** 033301
[141] de Sousa R and Das Sarma S 2003 *Phys. Rev.* B **68** 115322
[142] Marquardt F and Abalmassov V A 2004 *Preprint* cond-mat/0404749
[143] Erlingsson S I and Nazarov Yu V 2004 *Phys. Rev.* B **70** 205327
[144] Coish W A and Loss D 2004 *Phys. Rev.* B **70** 195340
[145] de Sousa R, Shenvi N and Whaley K B 2004 *Preprint* cond-mat/0406090
[146] Schliemann J, Khaetskii A and Loss D 2003 *J. Phys.: Condens. Matter* **15** R1809
[147] Vagner I D 2004 *HAIT J. Sci. Eng.* **1** 152 (*Preprint* cond-mat/0403087)
[148] Yuzbashyan E A, Altshuler B L, Kuznetsov V B and Enolskii V Z 2004 *Preprint* cond-mat/0407501
[149] Elliott R J 1954 *Phys. Rev.* **96** 266
[150] Rashba E I 1960 *Fiz. Tverd. Tela (Leningrad)* **2** 1224
Rashba E I 1960 *Sov. Phys.—Solid State* **2** 1109 (Engl. Transl.)
[151] Dresselhaus G 1955 *Phys. Rev.* **100** 580
[152] D'yakonov M I and Kachorovskii V Yu 1986 *Sov. Phys.—Semicond.* **20** 110
[153] Bonesteel N E, Stepanenko D and DiVincenzo D P 2001 *Phys. Rev. Lett.* **87** 207901
[154] Burkard G and Loss D 2002 *Phys. Rev. Lett.* **88** 047903
[155] Stepanenko D, Bonesteel N E, DiVincenzo D P, Burkard G and Loss D 2003 *Phys. Rev.* B **68** 115306

[156] Semenov Y G and Kim K W 2004 *Phys. Rev. Lett.* **92** 026601
[157] Pines D, Bardeen J and Slichter C P 1957 *Phys. Rev.* **106** 489
[158] Klauder J R and Anderson P W 1962 *Phys. Rev.* **125** 912
[159] Deng C and Hu X 2004 *Preprint* cond-mat/0406478
[160] Stoneham A M 1975 *Theory of Defects in Solids* (Oxford: Clarendon) p 455
[161] Bracker A S *et al* 2004 *Preprint* cond-mat/0408466
[162] Smet J H, Deutschmann R A, Ertl F, Wegscheider W, Abstreiter G and von Klitzing K 2002 *Nature* **415** 281
[163] Imamoğlu A, Knill E, Tian L and Zoller P 2003 *Phys. Rev. Lett.* **91** 017402
[164] Taylor J M, Marcus C M and Lukin M D 2003 *Phys. Rev. Lett.* **90** 206803
[165] Taylor J M, Imamoğlu A and Lukin M D 2003 *Phys. Rev. Lett.* **91** 246802
[166] Taylor J M, Giedke G, Christ H, Paredes B, Cirac J I, Zoller P, Lukin M D and Imamoğlu A 2004 *Preprint* cond-mat/0407640
[167] Schleser R, Ruh E, Ihn T, Ensslin K, Driscoll D C and Gossard A C 2004 *Appl. Phys. Lett.* **85** 2005
[168] Field M, Smith C G, Pepper M, Ritchie D A, Frost J E F, Jones G A C and Hasko D G 1993 *Phys. Rev. Lett.* **70** 1311
[169] Kouwenhoven L P, Schön G and Sohn L L 1997 *Proc. ASI on Mesoscopic Electron Transport* ed L L Sohn, L P Kouwenhoven and G Schön (Dordrecht: Kluwer)
[170] van der Wiel W G, De Franceschi S, Elzerman J M, Fujisawa T, Tarucha S and Kouwenhoven L P 2003 *Rev. Mod. Phys.* **75** 1
[171] Waugh F R, Berry M J, Mar D J, Westervelt R M, Campman K L and Gossard A C 1995 *Phys. Rev. Lett.* **75** 705
[172] Livermore C, Crouch C H, Westervelt R M, Campman K L and Gossard A C 1996 *Science* **274** 1332
[173] Jacak L, Hawrylak P and Wójs A 1998 *Quantum Dots* (Berlin: Springer)
[174] Tarucha S, Austing D G, Honda T, van der Hage R J and Kouwenhoven L P 1996 *Phys. Rev. Lett.* **77** 3613
[175] Bonadeo N H, Erland J, Gammon D, Park D, Katzer D S and Steel D G 1998 *Science* **282** 1473
[176] Gammon D, Bonadeo N H, Chen G, Erland J and Steel D G 2001 *Physica* E **9** 99
[177] Li X, Wu Y, Steel D, Gammon D, Stievater T H, Katzer D S, Park D, Piermarocchi C and Sham L J 2003 *Science* **301** 809
[178] Leonard D, Krishnamurthy M, Reaves C M, Denbaars S P and Petroff P M 1993 *Appl. Phys. Lett.* **63** 3203
[179] Eberl K, Lipinski M O, Manz Y M, Winter W, Jin-Phillipp N Y and Schmidt O G 2001 *Physica* E **9** 164
[180] Fricke M, Lorke A, Kotthaus J P, Medeiros-Ribeiro G and Petroff P M 1996 *Europhys. Lett.* **36** 197
[181] Lee H, Johnson J A, Speck J S and Petroff P M 2000 *J. Vac. Sci. Technol.* B **18** 2193
[182] Heidemeyer H, Denker U, Müller C and Schmidt O G 2003 *Phys. Rev. Lett.* **91** 196103
[183] Schedelbeck G, Wegscheider W, Bichler M and Abstreiter G 1997 *Science* **278** 1792
[184] Alivisatos A P 1996 *Science* **271** 933
[185] Ouyang M and Awschalom D D 2003 *Science* **301** 1074
[186] Meier F, Cerletti V, Gywat O, Loss D and Awschalom D D 2004 *Phys. Rev.* B **69** 195315
[187] Drexler H, Leonard D, Hansen W, Kotthaus J P and Petroff P M 1994 *Phys. Rev. Lett.* **73** 2252
[188] Warburton R J, Schäflein C, Haft D, Bickel F, Lorke A, Karrai K, Garcia J M, Schoenfeld W and Petroff P M 2000 *Nature* **405** 926
[189] Ciorga M, Sachrajda A S, Hawrylak P, Gould C, Zawadzki P, Jullian S, Feng Y and Wasilewski Z 2000 *Phys. Rev.* B **61** R16315
[190] Elzerman J M, Hanson R, Greidanus J S, Willems van Beveren L H, De Franceschi S, Vandersypen L M K, Tarucha S and Kouwenhoven L P 2003 *Phys. Rev.* B **67** 161308(R)
[191] Pioro-Ladrière M, Ciorga M, Lapointe J, Zawadzki P, Korkusiński M, Hawrylak P and Sachrajda A S 2003 *Phys. Rev. Lett.* **91** 026803
[192] Petta J R, Johnson A C, Marcus C M, Hanson M P and Gossard A C 2004 *Phys. Rev. Lett.* **93** 186802
[193] Fock V 1928 *Z. Phys.* **47** 446
Darwin C 1930 *Proc. Camb. Phil. Soc.* **27** 86
[194] Raymond S *et al* 2004 *Phys. Rev. Lett.* **92** 187402
[195] Fujisawa T, Austing D G, Tokura Y, Hirayama Y and Tarucha S 2002 *Nature* **419** 278
[196] Petta J R, Johnson A C, Yacoby A, Marcus C M, Hanson M P and Gossard A C 2004 *Preprint* cond-mat/0412048
[197] Hanson R, Willems van Beveren, Vink I T, Elzerman J M, Naber W J M, Koppens F H L, Kouwenhoven L P and Vandersypen L M K 2004 *Preprint* cond-mat/0412768
[198] Hanson R, Witkamp B, Vandersypen L M K, Willems van Beveren L H, Elzerman J M and Kouwenhoven L P 2003 *Phys. Rev. Lett.* **91** 196802
[199] Elzerman J M, Hanson R, van Beveren L H W, Witkamp B, Vandersypen L M K and Kouwenhoven L P 2004 *Nature* **430** 431
[200] Recher P, Sukhorukov E V and Loss D 2000 *Phys. Rev. Lett.* **85** 1962
[201] Kroutvar M, Ducommun Y, Heiss D, Bichler M, Schuh D, Abstreiter G and Finley J J 2004 *Nature* **432** 81
[202] Feher G 1959 *Phys. Rev.* **114** 1219
[203] Gordon J P and Bowers K D 1958 *Phys. Rev. Lett.* **1** 368
[204] Tyryshkin A M, Lyon S A, Astashkin A V and Raitsimring A M 2003 *Phys. Rev.* B **68** 193207
[205] Abe E, Itoh K M, Isoya J and Yamasaki S 2004 *Phys. Rev.* B **70** 033204
[206] Gupta J A, Awschalom D D, Peng X and Alivisatos A P 1999 *Phys. Rev.* B **59** R10421
[207] Chen P and Whaley K B 2004 *Phys. Rev.* B **70** 045311
[208] Epstein R J, Fuchs D T, Schoenfeld W V, Petroff P M and Awschalom D D 2001 *Appl. Phys. Lett.* **78** 733
[209] Engel H-A, Golovach V N, Loss D, Vandersypen L M K, Elzerman J M, Hanson R and Kouwenhoven L P 2004 *Phys. Rev. Lett.* **93** 106804
[210] Engel H-A, Kouwenhoven L P, Loss D and Marcus C M 2004 *Quantum Inf. Process.* **3** 115 (*Preprint* cond-mat/0409294)
[211] Folk J A, Potok R M, Marcus C M and Umansky V 2003 *Science* **299** 679
[212] Potok R M, Folk J A, Marcus C M, Umansky V, Hanson M and Gossard A C 2003 *Phys. Rev. Lett.* **91** 016802
[213] Cortez S, Krebs O, Laurent S, Senes M, Marie X, Voisin P, Ferreira R, Bastard G, Gérard J-M and Amand T 2002 *Phys. Rev. Lett.* **89** 207401
[214] Shabaev A, Efros Al L, Gammon D and Merkulov I A 2003 *Phys. Rev.* B **68** 201305(R)
[215] Engel H-A and Loss D 2001 *Phys. Rev. Lett.* **86** 4648
[216] Engel H-A and Loss D 2002 *Phys. Rev.* B **65** 195321
[217] Potok R M, Folk J A, Marcus C M and Umansky V 2002 *Phys. Rev. Lett.* **89** 266602
[218] D'yakonov M I and Perel' V I 1984 *Optical Orientation, Modern Problems in Condensed Matter Sciences* vol 8, ed F Meyer and B P Zakharchenya (Amsterdam: North-Holland)
[219] Wu Y, Fan R and Yang P 2002 *Nano Lett.* **2** 83
[220] Björk M T, Ohlsson B J, Sass T, Persson A I, Thelander C, Magnusson M H, Deppert K, Wallenberg L R and Samuelson L 2002 *Nano Lett.* **2** 87
[221] Gudiksen M S, Lauhon L J, Wang J, Smith D C and Lieber C M 2002 *Nature* **415** 617
[222] Grundmann M *et al* 1995 *Phys. Rev. Lett.* **74** 4043
[223] For review articles, see, e.g. Zrenner A 2000 *J. Chem. Phys.* **112** 7790
Gammon D and Steel D G 2002 *Phys. Today* **55** (10) 36
[224] Högele A *et al* 2004 *Preprint* cond-mat/0410506

[225] Baier M, Findeis F, Zrenner A, Bichler M and Abstreiter G 2001 *Phys. Rev.* B **64** 195326
[226] Gywat O, Engel H-A, Loss D, Epstein R J, Mendoza F M and Awschalom D D 2004 *Phys. Rev.* B **69** 205303
[227] Flissikowski T, Akimov I A, Hundt A and Henneberger F 2003 *Phys. Rev.* B **68** 161309(R)
[228] Martin I, Mozyrsky D and Jiang H W 2003 *Phys. Rev. Lett.* **90** 018301
[229] Gywat O, Engel H-A and Loss D 2004 *J. Supercond.* at press (Gywat O, Engel, H-A and Loss D 2004 *Preprint* cond-mat/0408451)
[230] Salis G, Kato Y, Ensslin K, Driscoll D C, Gossard A C and Awschalom D D 2001 *Nature* **414** 619
[231] Kato Y, Myers R C, Driscoll D C, Gossard A C, Levy J and Awschalom D D 2003 *Science* **299** 1201
[232] Kato Y, Myers R C, Gossard A C and Awschalom D D 2004 *Nature* **427** 50
[233] Chen P, Piermarocchi C, Sham L J, Gammon D and Steel D G 2004 *Phys. Rev.* B **69** 075320
[234] Calarco T, Datta A, Fedichev P, Pazy E and Zoller P 2003 *Phys. Rev.* A **68** 012310
[235] Bergmann K, Theuer H and Shore B W 1998 *Rev. Mod. Phys.* **70** 1003
[236] Sukhorukov E V and Loss D 1998 *Phys. Rev. Lett.* **80** 4959
[237] Sukhorukov E V, Burkard G and Loss D 2001 *Phys. Rev.* B **63** 125315
[238] Golovach V N and Loss D 2004 *Phys. Rev.* B **69** 245327
[239] Choi M-S, Bruder C and Loss D 2000 *Phys. Rev.* B **62** 13569
[240] Hatano T, Stopa M, Yamaguchi T, Ota T, Yamada K and Tarucha S 2004 *Phys. Rev. Lett.* **93** 066806
[241] Kodera T, van der Wiel W G, Ono K, Sasaki S, Fujisawa T and Tarucha S 2004 *Physica* E **22** 518
[242] Kodera T, van der Wiel W G, Maruyama T, Hirayama Y and Tarucha S 2005 *Fabrication and Characterization of Quantum Dot Single Electron Spin Resonance Devices* (Singapore: World Scientific Publishing) at press